Hindawi
International Journal of Intelligent Systems
Volume 2023, Article ID 8460498, 32 pages
https://doi.org/10.1155/2023/8460498

Research Article

Online Adaptive Neurochaotic Fuzzy Controller Design to Reduce the Seismic Response of Buildings Equipped with Active Tuned Mass Damper System

Ommegolsoum Jafarzadeh,[1] **Seyyed Arash Mousavi Ghasemi**,[1] **Seyed Mehdi Zahrai**,[2] **Ardashir Mohammadzadeh**,[3] **and Ramin Vafaei Poursorkhabi**[1]

[1]*Department of Civil Engineering, Tabriz Branch, Islamic Azad University, Tabriz, Iran*
[2]*School of Civil Engineering, College of Engineering, University of Tehran, Tehran, Iran*
[3]*Department of Electrical Engineering, University of Bonab, Bonab, Iran*

Correspondence should be addressed to Seyyed Arash Mousavi Ghasemi; amousavi2000@iaut.ac.ir

Received 28 October 2022; Revised 1 August 2023; Accepted 4 September 2023; Published 30 September 2023

Academic Editor: Surya Prakash

This paper presents a novel adaptive neurochaotic fuzzy control system based on type-2 fuzzy systems to reduce seismic responses in multistory structures with active tuned mass dampers under near-field and far-field earthquakes. In this proposed control system, the whole parameters of the plant are assumed to be completely unknown, the structural model is estimated using a multilayer perceptron neural network, and the system's Jacobian is extracted. The online estimation model is used, and the controller parameters are adaptively trained using the extended Kalman filter and error back-propagation method. Subsequently, the control force is applied to the active tuned mass damper, and the control objectives are met. The adaptive controller does not require initial settings, and a fractional-order proportional-integral-derivative controller is added to maximize stability and robustness against seismic vibration. A simple adaptive controller optimized by a particle swarm is also presented as an innovation. Comparing the performance of the improved simple adaptive controller and adaptive neurochaotic fuzzy controller, the proposed controllers appear more efficient and accurate. However, the superiority of the novel adaptive neurochaotic fuzzy over the improved simple adaptive controller in reducing maximum displacement, acceleration, drift, and base shear while maintaining acceptable performance under parametric uncertainties and seismic conditions is substantial.

1. Introduction

Natural disasters are considered the primary concern of civil engineers nowadays as they cause considerable damage to residents and structures [1–9]. In addition, the casualties and economic losses resulting from large-scale earthquakes and strong winds are remarkable [10]. To overcome these problems, structural control is a beneficial approach that minimizes the dynamic responses and excessive damage to the structures. Besides, the control strategies offer remarkable safety to the residents, raise the structural system's flexibility, and minimize the materials' usage [11]. Notably, many control systems were proposed to protect against excessive vibrations in an earthquake or wind excitation. Passive control systems [12, 13], semiactive control systems [14], active control systems [15–19], and hybrid control systems [20, 21] are typical examples of these systems. The active control systems have acceptable performance and adaptability for various excitation frequencies. These characteristics indicate the benefit of active control systems over passive control systems. These systems are helpful for transitive vibrations and minimizing the response to strong earthquakes. Furthermore, the semiactive and hybrid control strategies that seem more practicable for implementation rely on active control algorithms [22–24]. One of the passive control systems is the tuned mass damper (TMD),

which has received much attention so far [25, 26]. For example, Zamani and Etedali propose new formulas for optimal adjustment of tuned mass damper (TMD) parameters using a genetic programming method for seismically excited structures. The formulas use the teaching-learning-based optimization (TLBO) algorithm and derive high accuracy and efficiency. Numerical studies show that these formulas are efficient for seismic control applications, reducing floor displacement and absolute acceleration [27]. Among several passive devices for structural control applications [28–30], a family of extremely nonlinear dampers (particle dampers) that concurrently exploit momentum transfer and internal energy dissipation provides some benefits in practical settings. Particle dampers, which developed from the single-particle impact damper [31], are containers or structural spaces partly filled with particles (e.g., ball bearings, tungsten powders, etc.) [32].

The main disadvantage of this passive control strategy is that it is limited to a narrow frequency band. Additionally, since this strategy is entirely sensitive to parameter tuning, a characteristic structural frequency needs to be considered for tuning. Basically, severe earthquakes or strong winds lead to irreparable damage to the structures and change their dominant frequency. Therefore, due to the sensitivity of the TMD damper optimal parameters to the dominant frequency of the structure or ignoring the effect of soil-structure interaction, it leads to an unwanted bad shock absorption effect [25, 33–35]. To overcome the above-mentioned problems associated with TMDs, many studies have proposed using several TMDs with different properties [36–40]. However, an active tuned mass damper (ATMD) is a more practical strategy because it is applicable considering several vibration states and is a useful control approach for multistory structures [41]. This system uses a relatively small mass to minimize the structures' response and enhance performance [42]. Furthermore, the active control force employed to transmit this small mass exerts a secondary inertial force against the vibrations [43]. Although, concerning the building and the mass of the adjustable damper, which constitutes the mass of the entire system, the high level of driving force requirements might be utilized for the ATMD systems and put the whole control system in an unstable condition. Recent years have seen various control algorithms for improving the ATMD control's performance because the control systems' performance is significantly related to the control algorithm that tunes the control force. In this case, the structure's dynamic vibrations are minimized, which improves the safety and performance of civil engineering structures under strong environmental excitations. Besides, a suitable trade-off is created between these conflicting purposes, such as reducing the control force and structural responses [44, 45]. LQR [46–48], H2 and H∞ [49, 50], bang-bang control [51], acceleration feedback regulators [52, 53], feedforward and feedback optimal tracking controller (FFOTC) [54], sliding mode control (SMC) [55–57], fuzzy PID controller [58, 59], and PID controller [48, 60, 61] are the significant algorithms mainly used for adjusting the control force used in ATMD. In fact, choosing an effective control algorithm is a determent factor that raises the control system's efficiency [62]. The control algorithms that have been presented so far can deliver a large number of benefits based on their characteristic practicalities and purposes.

Semiactive control of base-isolated structures has been well studied in recent years. However, there is a study gap in the assessment of the structure in the literature. Etedali and Zamani carry out research on semiactive control of nonlinear smart base-isolated structures using an MR damper for the case of controlled ones in both passive-off and passive-on modes and also tuning the command voltage of the MR dampers by a multiobjective modified clipped optimal controller [63]. In the study by Zamani and Etedali, a new framework controller based on energy concepts, namely OIT2FOFPIDC, was developed for implementation in seismically excited structures [64]. However, this model was not investigated for active seismic control of structures with tuned mass dampers or tendon systems. In addition, the effectiveness of the model for bridges and tall buildings exposed to strong wind can also be discussed. A simple and useful controller based on the optimal output feedback controller for use in tall structures equipped with smart base-isolated was developed by Zamani and Etedali [65]. The main motivation of in research is to propose a new framework of multiobjective brain emotional learning-based intelligent controller for tuning the command voltage of MR dampers in real time for smart base-isolated structures.

It is noteworthy that the previous decades have seen many studies conducted regarding the fuzzy logic controller (FLC) [39, 43, 66, 67], and this strategy has been considered a control algorithm for the structures' active control. Faravelli and Yao were the pioneers in this field and proposed a set of instructions to perform the active control strategy with FLC in the structures [68]. After that, the active control method's application in the benchmark buildings [69] using an FLC was examined by Al-Dawod in 2004 [70]. The FLC is designed based on human knowledge and experience to create the rules of control and outline membership functions. Besides, human knowledge is limited for solving complex problems and cannot lead to efficient control responses for a specific structure. To overcome these drawbacks, the control systems' parameters need to be fundamentally adjusted with optimization algorithms [62, 71–76]. Structural control studies primarily focus on nominal parameters, but real structures face uncertain responses due to simplifications in engineering models, estimates, assumptions, and unpredictable environmental loads. So, natural disasters like strong winds and earthquakes cause damage to structures. Stiffness, natural frequencies, and mode shape variations are the major parameters that have an adverse effect on the structures' properties. These uncertainties lead to losing the effective performance of the controller in reducing the structure's seismic responses. In this case, the control systems are set offline by algorithms, possibly destabilizing them [77–79]. Thus, a fundamental need is to propose a control strategy that is not sensitive to parametric changes and has remarkable performance for structural control. Accordingly, adaptive intelligent control algorithms have been introduced as a promising approach

and suitable alternative to traditional model-based control algorithms [80]. The effective control of nonlinear, time-varying, and time-delayed complicated structures is obtained through these algorithms based on artificial intelligence [81] and soft computing techniques. The structural system's specifications are assessed under severe earthquakes in real time. In order to minimize the dynamic responses, suitable control forces are applied to the structure that also compensates for the probable damage in the structure [55, 82–85].

Type-1 fuzzy logic has been implemented in different studies; however, its capability for modeling uncertainties is being questioned. On the other hand, type-2 fuzzy systems have received much attention compared to type-1 ones since they model more uncertainties with the minimum rules [86–88].

Therefore, type-2 fuzzy logic was introduced, which is created by fuzzification of the secondary membership functions. On the other hand, the information processing speed in type-2 fuzzy systems is low because they contain many embedded type-1 fuzzy sets, which increases the theoretical and computational complexities in inference operators and type reduction. Interestingly, the remarkable capabilities of type-2 fuzzy systems in modeling uncertainties outweigh such challenges. Notably, several studies [80, 89–93] presented methods for increasing the type-2 fuzzy system's computation speed. In addition, interval type-2 fuzzy systems have been significantly employed in many fields, such as modeling nonlinear systems [94], system identification [95], time series prediction [96], and intelligent control [97].

In 2018, Golnargesi et al. exploited the IT2FLC in ATMD to control the response of a structure according to soil-structure interaction and achieved acceptable results [98]. In a significant study in 2020 associated with IT2FLC, Hosseini Lavassani and Shangapour presented the applicability of this strategy in the hybrid control of the behavior of a real high-rise burning building according to the soil-structure interaction. The hybrid control method included TMD and a magnetorheological (MR) damper, and the parameters were adjusted offline [99]. In 2021, Hadad Baygi and Seyed Mahdi analyzed a four-story structure subjected to a shaking table, integrating proportional-integral-derivative and FLC. The primary objective of this study was to minimize the isolation system's displacement, assuming that the superstructure's acceleration did not rise for far-field and near-field earthquake events [90]. Besides, a simple adaptive controller (SAC), which has a good performance, was examined by Soares et al. for attenuating the bridge's seismic responses against parametric uncertainties [100]. In another study by Soares et al., the neurofuzzy controller was combined with SAC and applied to the cable-stayed bridge subjected to central US seismic excitations, and acceptable results were presented [10].

It is worth mentioning that the brain's performance in fuzzification and approximate reasoning when facing uncertainties is considered for the theory of fuzzy sets [101]. Hence, using the operational and structural features of the brain can tackle the challenges of fuzzy systems. According to neuron studies, chaotic dynamics are one of the remarkable characteristics of the brain. Using chaotic dynamics, the brain can cover a wide range of behaviors and quickly process massive amounts of data [102, 103]. Therefore, the integration of fuzzy systems and chaos theory can be strikingly beneficial since more efficacious performance is obtained from the brain to understand and realize the phenomena. Also, this new system has a remarkable performance in fuzzification and approximate reasoning in the fuzzy sets' theories and can create chaotic dynamics in the chaos theory. The research in this field is divided into two classes: chaotic fuzzy systems (like fuzzy systems for modeling chaotic systems [104] and chaos control [105]) and the combination of the chaotic mappings with fuzzy sets, namely chaotic fuzzy sets [105, 106].

Moreover, fuzzy systems can be combined with the neural network to maximize the efficiency of the control strategy in the structures [91]. In this case, learning algorithms need to be applied to enhance the neural network's performance and adjust the fuzzy system's parameters [10, 107]. Hence, the rules considered for the fuzzy systems are automatically analyzed in the systems, and the control system's speed is considerably enhanced. For instance, Wang and Kumbasar employed big bang-big crunch (BBBC) optimization and particle swarm optimization (PSO) to optimize interval type-2 fuzzy neural networks' parameters [108]. A more practical strategy, namely semiactive seismic control, was introduced by Bozorgvar and Zahrai in 2019. Also, a magnetorheological (MR) damper was utilized to improve seismic behavior in a three-story building. Additionally, an adaptive neural-fuzzy intelligent controller was considered to specify the damper input voltage. Using a genetic algorithm, the controller's performance became efficient [109]. Furthermore, Tavoosi et al. proposed an adaptive inverse type-2 fuzzy neural controller as a novel approach for online controlling nonlinear dynamical systems [110].

A foundation for interval-valued Type-2 (IT2) Gaussian fuzzy sets with finite range is presented by Tolga et al. (2020). Undoubtedly, all vague analyses, methods, and complex problems can be addressed with the FIT2 Gaussian fuzzy numbers and their arithmetic [111]. Considering the effect of SSI, Nazarimofard et al. (2018) obtained a mathematical model to obtain the seismic performance of irregular multistory buildings with two active tuned mass dampers (ATMDs) at the center of mass on the top floor. They investigated the seismic response of buildings with asymmetric floor plans [16]. According to Zamani and Etedali, ROFBANFISC is a robust output feedback-based ANFIS controller. Different soil types are used to validate the robustness of the OOFC and ROFBANFISC. Considering six performance criteria, a 40-story structure subjected to five real ground motions is numerically examined. Compared to the OOFC, ROFBANFISC is more robust under various soil conditions [112]. Sabetahd proposed a robust adaptive controller for use in the active tuned mass damper (ATMD) system for addressing undesirable vibrations in multistory buildings under seismic conditions. An online adaptive type-2 neural-fuzzy controller (AT2NF) is presented [113].

The presentation by Kousoloukas et al. focused on developing control variants for mass damper schemes on building-like structures. Sixty-three percent refer to passive-tuned mass dampers, 31 percent to hybrid mass dampers, four percent to active mass dampers, and only two percent to semiactive mass dampers [114]. Through various examples with real data, Mohammadzadeh proposed various methods for optimizing interval Type-2 fuzzy systems. Gradient descent, the Kalman filter, and the genetic algorithm will be used for training, and error back-propagation will be used for optimization [115].

According to the explanations above, combining fuzzy systems, chaotic theory, and neural networks with a practical optimization method or suitable algorithm can provide unique benefits. On the other hand, no study has presented a control strategy that can be effective for many applications. In the cutting-edge paper of 2010, Wong et al. proposed a new model called the Lee-Oscillatory Chaotic Fuzzy Model (LOCFM). This study integrated chaos and fuzzy theories using a chaotic neuron model, namely the improved Lee-Oscillatory [116]. According to this study, chaotic fuzzy sets have an advantageous control strategy to model the maximum number of uncertainties. Although this approach is interesting, the studies suffer from several gaps and shortcomings. In light of recent events in the chaotic fuzzy system, there is now considerable concern about the practicality and authenticity of the results. However, using ATMD and the adaptive form of this control strategy can overcome such pitfalls and concerns. Despite this interest, to the best of our knowledge, no one has presented an adaptive neurochaotic fuzzy (ANCF) system to control and minimize responses in the structural system containing ATMD. The current study was conducted based on the fuzzy approach and inspired by the brain's capabilities in creating various dynamics, fast information processing, and the modified Lee-Oscillator structure. Thus, a novel fuzzy set, namely the adaptive neurochaotic fuzzy sets, is presented here as a controller, and this control strategy is based on the type-2 fuzzy systems.

In this study, we propose an approach to reduce the structure's dynamic responses in near-field and far-field earthquakes without considering the structural system's dynamics and input information of the event. In order to derive the Jacobian and predict the structural system model, a multilayer perceptron (MLP) neural network structure is employed. In addition, the coefficients of the MLP are considered adaptive, so their parameters can be used to estimate the model parameters accurately. The ATMD is subjected to a controlled force tuned through the optimized controller parameters by utilizing the extended Kalman filter and the error back-propagation method. As a result, the adaptive control system employed in this study operates online. In particular, the roof displacement is considered the control error signal, which must be minimized. As part of the neurochaotic fuzzy system controller, a fractional-order proportional-integral-derivative (FOPID) is added to maximize its stability and resistance to seismic vibrations. Furthermore, the performance of the ANCF controller is evaluated based on an adaptive control model based on the simple adaptive controller optimized by PSO. In this study, the improved controller is referred to as the ISAC controller. To achieve the control gains required for specifying the considered interactions in a control system, the ISAC controller does not require the complete identification of the parameters of the controlled system. An adaptive type-2 neural-fuzzy controller (AT2NF) was proposed in the previous work to mitigate unwanted vibrations in an 11-story building [113]. This study is noteworthy for its proposed state-of-the-art controller, which optimizes the parameters of SAC online via PSO. In contrast to the previous paper, this paper features a remarkable level of accuracy and ability to maintain acceptable performance during operation. According to the results of the related studies, the control strategies are divided into two categories: (1) the system dynamics are known, and the controller is designed online. (2) The system dynamics are assumed to be unknown, and the controller is designed offline. Hence, evolutionary algorithms can be used to optimize the controllers, and optimized parameters are applied to the system. In fact, the system parameters are assumed to be implicitly known. The disadvantages of these methods are their time-consuming nature and the fact that they may not achieve an optimal operating point, which increases the computational work and may lead to control instability. By comparing the results, it can be concluded that the ANCF controller has significant advantages when providing control functions. The major benefits of this controller compared to the previous studies are as follows:

(i) The structural system's dynamics are assumed to be uncertain, and an online scheme is used to design the controller.

(ii) Unlike previous study methods, the Jacobian of the plant is not needed, and the MLP neural network is considered for modeling and extracting the system's Jacobian.

(iii) Since the proposed strategy is adaptive, the controller does not require any initial settings to be considered.

(iv) The proposed strategy has enough capability to deal with a time-varying system and tackle uncertain parameters.

(v) An adaptive control strategy with the highest efficiency can be produced using a combination of chaotic theory, fuzzy theory, neural networks, and an optimization algorithm.

(vi) The remarkable capability of the proposed control strategy to create various fuzzy sets, such as type-1 or type-2 fuzzy sets, convex or nonconvex, is unique.

(vii) The performance of an adaptive neurochaotic fuzzy controller in a larger-scale structural system can be evaluated.

The rest of this paper is organized as follows: Section 2 mentions the equations of motion. Section 3 is devoted to the proposed control scheme. Section 4 is devoted to numerical analysis, structure specifications and dynamics, and earthquake site. Section 5 is devoted to results and discussion. Section 6 is devoted to the conclusion.

2. The Equations of Motion

This section gives the necessary equations associated with the motion in the structural model (see Figure 1). ATMD is installed on the highest floor, with N-degree-of-freedom (DOF) in the shear building, and the dynamic equation of motion has several characteristic equations that are as follows:

$$\mathrm{M}\ddot{x}(t) + \mathrm{C}\dot{x}(t) + \mathrm{K}x(t) = -M\Lambda\ddot{x}_g(t), \tag{1}$$

where $x(t)$ indicates the vectors considered for specifying the displacement in the structure, and the velocity is denoted by $\dot{x}(t)$, and $\ddot{x}(t)$ is the acceleration. Also, the excitation acceleration vector is $\ddot{x}_g(t)$ which is considered in the structure with dimensions $(N+1)\times 1$. Notably, the number of freedom degrees is characterized by N. Accordingly, M shows the mass matrices, C is used for indicating damping, and K the stiffness matrices of the structure equipped with an ATMD with dimensions represents $(N+1)\times(N+1)$. Furthermore, the $(N+1)\times 1$ relative displacement vector is highlighted through $X(t)$.

$$X(t) = \left[x_1(t), x_2(t), \ldots, x_i(t), \ldots, x_N(t), x_{\mathrm{TMD}}(t)\right]^T. \tag{2}$$

In relation to equation (2), the displacement of the i th story relative to the ground is represented by $x_i (i = 1, 2, \ldots, N)$. Also, the displacement between the TMD and the ground is indicated by the x_{TMD}. Assuming that the masses are accumulated at floor levels, the following mass matrix is considered:

$$M = \mathrm{diag}\left(m_1, m_2, \ldots, m_i, \ldots, m_N, m_{\mathrm{TMD}}\right), \tag{3}$$

where the mass of the i-th floor is indicated by $m_i (i = 1, 2, \ldots, N)$, and the mass of the TMD is shown by m_{TMD}. Adding a TMD to the primary structure leads to adding a degree of freedom to the structure. The structural stiffness matrix is shown in the following equation:

$$K = \begin{bmatrix} (k_1 + k_2) & -k_2 & & & \\ -k_2 & (k_2 + k_3) & -k_3 & 0 & \\ & \vdots & \vdots & & \\ & & & \vdots & \\ & & \mathrm{sym} & -k_N & (k_N + k_{\mathrm{TMD}}) & -k_{\mathrm{TMD}} \\ & & & & -k_{\mathrm{TMD}} & -k_{\mathrm{TMD}} \end{bmatrix}, \tag{4}$$

where the stiffness of the i-th floor is highlighted through $k_i (i = 1, 2, \ldots, N)$. Furthermore, k_{TMD} is employed to demonstrate the stiffness factor of the TMD. According to Rayleigh's method, the structural damping matrix C is assumed to be proportional to the mass and stiffness matrices, as shown in equation (5). Accordingly, ω_1 and ω_2 represent the natural structural frequencies in the first and second modes. In addition, ξ denotes the structural critical damping ratio in the first two modes.

$$C = \frac{2\xi\omega_1\omega_2}{\omega_1 + \omega_2} M + \frac{2\xi}{\omega_1 + \omega_2} K. \tag{5}$$

The highest floor contains a smart structure employing an active control system. There is an actuator between the structure and the TMD system. This actuator is used to apply a controlled force $u(t)$ to the ATMD in real time. Besides, its reaction is applied to the top floor. Accordingly, equation (6) shows the motion of the structure equipped with an ATMD.

$$\mathrm{M}\ddot{x}(t) + \mathrm{C}\dot{x}(t) + \mathrm{K}x(t) = -M\Lambda\ddot{x}_g(t) + \mathrm{D}u(t). \tag{6}$$

Concerning equation (6), the location vector of the control force is shown by vector D. This vector is based on the location of actuators. The highest floor is the location of ATMD, $D = [0, \ldots, 0, -1, 1]^T$ indicates the $(N+1)\times 1$ location vector of the control forces. As shown in equation (7), the standard state space form is specified for the dynamic equation of motion in which the vector $Z(t)$ is selected.

$$Z(t) = \begin{Bmatrix} x(t) \\ \dot{x}(t) \end{Bmatrix}. \tag{7}$$

Furthermore, the state matrix A, input matrix B, output matrix G, and vector H indicate

$$\begin{aligned} A &= \begin{bmatrix} 0 & I \\ -M^{-1}K & -M^{-1}C \end{bmatrix}, \\ B &= \begin{bmatrix} 0 \\ M^{-1}D \end{bmatrix}, \\ H &= \begin{bmatrix} 0 \\ -\Lambda \end{bmatrix}, \\ G &= [I\,0], \\ y(t) &= \mathrm{G}Z(t). \end{aligned} \tag{8}$$

Here, $y(t)$ denotes the output vector, and I and 0 are the identities and zero matrices with suitable dimensions. Notably, the matrix of B is employed to determine the control forces' locations. In other words, the controlling force is not

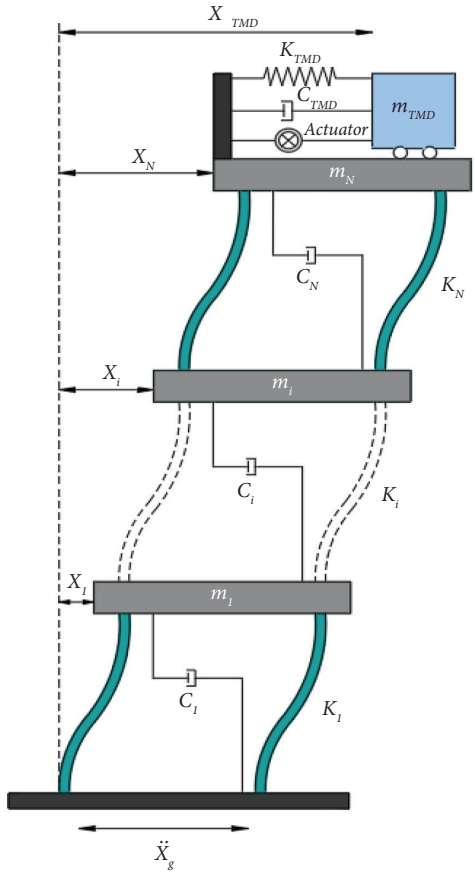

Figure 1: The condition of ATMD in the considered structure.

required to apply in every story. Due to modeling errors, nominal and real physical parameters of structures are different. Since the exact values of the elements of matrices M, C, and K in equation (1) are unknown, equation (9) illustrates it is reasonable to presume that their values are within certain intervals.

$$\begin{aligned} M &= (1+\Delta_M)\overline{M}, \\ C &= (1+\Delta_C)\overline{C}, \\ K &= (1+\Delta_K)\overline{K}. \end{aligned} \tag{9}$$

According to equation (9), the nominal values of M, C, and K are indicated by $\overline{M}, \overline{C}$, and $\overline{K}$. Also, the uncertainty percent of the structural model is represented by Δ_M, Δ_C, and Δ_K.

3. The Proposed Control Scheme

This section explains the control approach employed in this paper. In addition, the necessary information is given.

3.1. The MLP Neural Network Structure. Artificial neural networks (ANNs) are created based on the biological model of the human brain and have shown remarkable capabilities in solving many problems nowadays. The concept of the ANN is actually one of the main subbranches of artificial intelligence. The ANNs have features such as adaptive learning, self-organization, real-time operators, generalization, stability and flexibility, and parallel processing. Various neural network models and training algorithms make them useful in many applications, such as estimating functions, prediction, pattern recognition, and control. Another field in which neural networks are widely used is system identification. Identification aims to obtain an approximation of the dynamic models for designing the optimal controller without any information regarding the system dynamics.

In this study, a multilayer perceptron (MLP), one of the most important structures in the neural network (ANN) and has much applicability, is employed. The multilayer perceptron (MLP) neural network can approximate any nonlinear function with optimal accuracy. The MLP's remarkable ability to identify systems even with complex dynamics without explicit dependency on their model has increased the popularity of using neural networks for adaptive control. Overall, there are three types of neuron layers in the neural networks considered in this study, which are as follows: input layer, middle layer, and output layer.

According to Figure 2, the neural network's inputs are shown by $u(t-\tau_1), u(t-\tau_2), \ldots, u(t-\tau_n)$, and $\tau_1, \tau_2, \ldots, \tau_n$ are constant. The control signal is considered with the output system at the instant t, whose sum is represented by $u(t)$. Notably, $w_{11}^1, w_{12}^1, \ldots, w_{1n}^1$, the middle layer weights are related to the first neuron, and $w_{21}^1, w_{22}^1, \ldots,$ and w_{2n}^1 are considered for the second layer. The middle layer weights connected to neuron q are captured by $w_{h1}^1, w_{h2}^1, \ldots, w_{qn}^1$, in which q indicates the neuron's number. The output and neuron considered in the middle layer have the weights $w_{21}, w_{22}, \ldots, w_{2q}$.

The neural network's input is the control signal and system output at previous time samples. Then, the middle layer contains the neuron's output, which is computed through the following relations:

$$\begin{aligned} \text{net}_i &= w_i^1 U, \\ o_i &= g(\text{net}_i), \quad i = 1, \ldots, q, \end{aligned} \tag{10}$$

where

$$\begin{aligned} U &= \left[u(t-\tau_1), u(t-\tau_2), \ldots, u(t-\tau_n)\right]^T, \\ w_i^1 &= \left[w_{i1}^1, w_{i2}^1, \ldots, w_{\text{in}}^1\right], \\ g(\text{net}_i) &= \frac{1-\exp\ (-\text{net}_i)}{1+\exp\ (-\text{net}_i)}. \end{aligned} \tag{11}$$

The following equation gains the output of the MLP neural network:

$$y = w_2 O, \tag{12}$$

where

$$\begin{aligned} O &= \left[o_1, o_2, \ldots, o_q\right]^T, \\ w_2 &= \left[w_{21}, w_{22}, \ldots, w_{2q}\right]. \end{aligned} \tag{13}$$

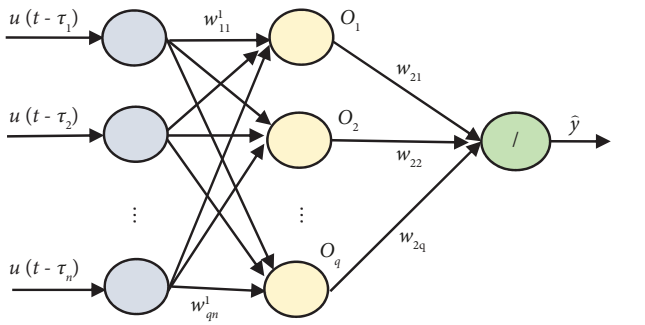

FIGURE 2: The structure of the MLP network.

With the aim of minimizing the cost function of E, the neural network's weights are trained.

$$E = \frac{1}{2}e_{\text{est}}^2 = \frac{1}{2}\left(y_d - \hat{y}\right)^2. \tag{14}$$

Concerning equation (14), the obtained output is specified by y_d, and the neural network's output is shown by $\hat{y}$.

Weights in step $t+1$ are $(t+1) = w(t) - \eta(\partial E/\partial w)$. Gradient descent and back-propagation errors are used for training. In order to obtain $(\partial E/\partial w)$, the chain differentiation of $(\partial E/\partial w) = (\partial E/\partial e)(\partial e/\partial \hat{y})(\partial \hat{y}/\partial w)$ applies. According to equation (15), the relations $(\partial E/\partial e) = e$, $(\partial e/\partial \hat{y}) = -1$, $(\partial \hat{y}/\partial w) = O$ are substituted, and the rule of training weights is computed. Equation (15) outlines the rule of training weights.

$$w_2(t+1) = w_2(t) + \eta_{\text{best}} O. \tag{15}$$

Equation (16) is considered to obtain the adaptive rule for the weights of the first layer.

$$w_i^1(t+1) = w_i^1(t) + \eta e_{\text{est}} g'\left(\text{net}_i\right) w_{2i} U, \tag{16}$$

where w_i^1 implies the vector of the weights neuron in the middle layer that is related to the i-th layer; besides, $g'(\text{net}_i)$ denotes the derivation of $g(\text{net}_i)$ according to net_i input. Notably, the training rate of gradient descent is shown by η. Concerning η, the adaptive rate is adjusted online.

3.2. The System Jacobian. Equation (17) illustrates the computation of the system's Jacobian employing the obtained model:

$$\frac{\partial \Delta f}{\partial u_c} = \left[w_{11}^1, w_{21}^1, \ldots, w_{q1}^1\right] \text{diag}\left(\left[g'(\text{net}_1), \ldots, g'\left(\text{net}_q\right)\right] w_2\right), \tag{17}$$

where $(\partial \Delta f/\partial u_c)$ represents the derivative of system output concerning the control input. Also, the diagonal vector of matrix A is shown by $\text{diag}(A)$. The expressions $[w_{11}^1, w_{21}^1, \ldots, w_{q1}^1]$, and $A = [g'(\text{net}_1), \ldots, g'(\text{net}_q)]$ are related to the vector of weights connected to the first input and neurons of the middle layer and the vector of the derivative of the output of neurons of the middle layer with respect to their input, respectively. The vector of weights connected to the output and neurons of the middle layer is indicated by w_2.

3.3. The Structure of Interval Type-2 Fuzzy Sets. In the groundbreaking paper of 1975, the IT2FS was proposed by Zadeh [117] and then developed and grown by Karnik et al. [118]. In fact, the type-2 fuzzy is the corrected form of the type-1 fuzzy, with the same fuzzy rules and membership function. The membership function of type-1 is a fixed number. While in type-2 it is a fuzzy set. The third dimension in the type-2 fuzzy set is used to model the uncertainties that type-1 fuzzy cannot model. Type-2 fuzzy is used when the system complexity is high [44, 45]. The continuous form of the IT2FSs is defined as follows:

$$\widetilde{A} = \left\{\left(x(x,u), \mu_{\widetilde{A}}(x,u)\right) \mid \forall_x \in X, \forall_u \in J_x \subseteq [0,1]\right\}, \tag{18}$$

where $0 \le \mu_{\widetilde{A}}(x,u) \le 1$, and $\widetilde{A}$ is also equal to $\int_{x\in X}\int_{u\in J_x}(\mu_{\widetilde{A}}(x,\text{u})/(x,u))$. Accordingly, $\int\int$ represents the union over whole admissible input variables x and u. Besides, the primary membership of x is denoted by $J_x \subseteq [0,1]$, and $\mu_{\widetilde{A}}(x,\text{u})$ indicates a type-1 fuzzy set known as the second set. Hence, in order to reduce the computation, an interval type fuzzy is employed, according to which $\mu_{\widetilde{A}}(x,u) = 1$.

Research indicates an increase in the ability of type-2 fuzzy sets to model more uncertainties. However, according to this pattern, (1) since each input must have multiple membership values, the number of type-1 fuzzy sets enclosed in these sets increases unnecessarily, (2) although these sets inherently include various fuzzy sets, such as convex and nonconvex, normal, abnormal, and binomial sets, none of them can be utilized alone in modeling uncertainties. Notably, only the lower and upper membership functions specified beforehand are employed to model the uncertainties. That issue unnecessarily increases the uncertainty interval, and (3) the upper and lower membership values are determined through mathematical equations. They are absolute values, which contradicts the fuzzy concept. Therefore, despite the undeniable capabilities of these sets in modeling uncertainties, the above features have caused type-2 fuzzy sets to encounter problems in practical and online applications. The main drawbacks to these collections are (1) increasing the complexity of the theory of these fuzzy sets, (2) significant reduction in information processing speed, and (3) lack of ability to create new membership functions or flexibility in selecting one or more membership functions enclosed in the uncertainty effect area. In order to tackle the limitations mentioned above and create novel and varied behaviors for the fuzzy membership values, the features of chaotic mappings are used.

3.4. The Neurochaotic Fuzzy Sets. The neurochaotic fuzzy sets are modeled as a single-layer recurrent neural network with an input neuron, an output neuron, and three hidden neurons, as shown in Figure 3. The mapping between the input and output is defined as follows [119]:

$$\begin{aligned} u(n+1) &= f\left(a_1 u(n) - a_2 v(n) + a_3 z(n) + a_4 x - \theta_u\right), \\ v(n+1) &= f\left(b_3 z(n) - b_1 u(n) + b_2 v(n) + b_4 x - \theta_v\right), \\ w(n) &= \mu_A(x), \\ z(n+1) &= \max\ (0, \min\ (1, \left(u(n+1-v(n+1)) \times \exp\left(-K\left(x - m_A\right)^2\right) + w(n)\right), \end{aligned} \tag{19}$$

where u, v, w, and z show the modes of the stimulator, inhibitor, input, and output neurons, respectively. The membership function and the average value of the fuzzy set A are indicated by m_A and $\mu_A(x)$; a_{1to4} and b_{1to4} are considered the neurons' weights; the bias of stimulating and inhibitor neurons is shown by θ_u and θ_v; K is the latency constant, and x is the input value; $f()$ indicates the function of the stimulator neuron, and $0 \le \mu_A(x) \le 1$.

When the above mapping uses x as the bifurcation parameter, the chaotic set can be obtained by the bifurcation diagram of the mapping in equation (19)

For example, if θ_u and θ_v were zero in equation (19), $\mu_A(x)$ and $f(x)$ would be defined as follows:

$$\begin{aligned} \mu_A(x) &= \exp\ \left(-\frac{(x-\mu)^2}{2\sigma^2}\right), \\ f(x) &= \exp\ \left(-x^2\right). \end{aligned} \tag{20}$$

In this case, the bifurcation diagram is in equation (19), used to represent the neurochaotic fuzzy membership functions in parameter changing.

3.5. The Neurochaotic Fuzzy Controller Structure. This paper considers the neurochaotic fuzzy controller structure as a novel control strategy. Fuzzy systems, chaotic theory, and neural networks indicate aspects of the human brain's information-processing mechanism and decision-making [101, 102]. Hence, combining these sciences can create a robust system with fuzzy reasoning, self-adaptation, and chaotic search capabilities. Since the novel behaviors originate from the chaotic mappings, the chaotic theory is combined with the fuzzy theory. Furthermore, combining the neural network with the chaotic and fuzzy theories eliminated the fuzzy rules and made the control strategy adaptive. Using a suitable optimization method or algorithm can also enhance the neural network's capability. Therefore, the chaotic neural-fuzzy controller structure along with the extended Kalman filter is considered for optimizing the performance of the type-2 neural-fuzzy controller.

Since the membership function proposed in equation (19) can create the interval type-2 fuzzy sets, the neurochaotic fuzzy systems (NCFSs), similar to the interval type-2 fuzzy neural network (IT2FNN) system, are proposed. The main difference between these systems is calculating the higher and lower membership degrees. The higher and lower membership degrees are specified through a certain and fixed mathematical formula in IT2FNN. In comparison, this calculation is conducted based on the mapping rules in the neurochaotic fuzzy system. Hence, the higher and lower membership values change according to the chaotic mapping and input value parameters. As shown in Figure 4, the structure of the neurochaotic fuzzy system consists of five layers. The input nodes are shown in the first layer. The higher and lower membership values are computed in the second layer. The calculations concerning the fuzzy rules are conducted in the third layer. The reduced and final outputs are calculated in the fourth and fifth layers, respectively.

The if-then rule can be defined as follows:

$$R^i\text{: IF } x_1 \text{ is } F_1^i, \text{and} \ldots, \text{and } x_n \text{ is } F_n^i, \text{THEN } y^i \text{ is } Y^i, \tag{21}$$

where $i = 1, 2, \ldots, M$ shows the number of rules, and F_1^i is the neurochaotic fuzzy membership function in the front section. The set of centers of the neurochaotic fuzzy membership function of output is represented by $Y^i = [y_l^i, y_r^i]$. The intensity of each rule is represented by $F^i = [f^i, \overline{f}^i]$; so that the values which f^i and $\overline{f}^i$ are calculated by $\prod_{j=1}^{n} \mu_{\breve{F}_j^i}(x_j)$ and $\prod_{j=1}^{n} \overline{\mu}_{\breve{F}_j^i}(x_j)$. In order to calculate the final output y, the reduced output values ($[y_l, y_r]$) is obtained through the Karnik–Mendel algorithm and the following equations [120]:

$$y_l = \frac{\sum_{i=1}^{L} \overline{f}^i y_l^i + \sum_{j=l+1}^{M} f^i y_l^j}{\sum_{i=1}^{L} \overline{f}^i + \sum_{i=l+1}^{M} f^i}, \tag{22}$$

$$y_r = \frac{\sum_{i=1}^{R} \overline{f}^i y_r^i + \sum_{j=R+1}^{M} \overline{f}^j y_r^j}{\sum_{i=1}^{R} f^i + \sum_{j=R+1}^{M} \overline{f}^j}, \tag{23}$$

where L and R are the switch points from the bottom to the top membership function and vice versa, and these parameters are calculated by using the Karnik–Mendel algorithm. Finally, the final output value is computed through $y = (y_l + y_r)/2$.

3.6. The Extended Kalman Filter and Error Back-Propagation. The training weights based on the error back-propagation and the extended Kalman filter are employed in the current study. When the roof displacement is minimized, the optimal response is achieved. At first, the square error at any moment is calculated between the desirable response and the network output at instant t:

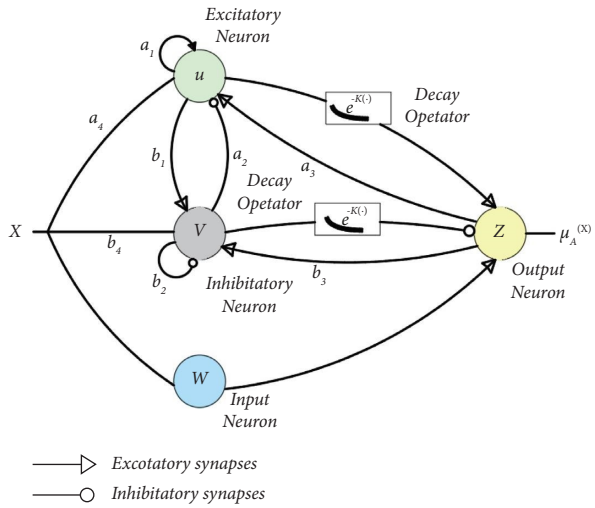

Figure 3: The generative structure of a neurochaotic fuzzy set.

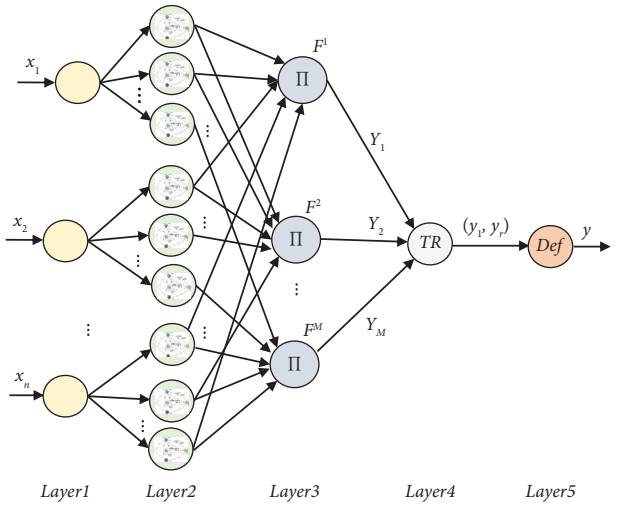

Figure 4: The structure of the neurochaotic fuzzy system.

$$E = \frac{1}{2},$$
$$e^2 = \frac{1}{2}(\Delta f)^2. \tag{24}$$

The displacement of the roof in the x-axis is considered as a control error in equation (24), which is represented by e. According to the training principle of the error back-propagation and the extended Kalman filter, the parameters of the neurochaotic fuzzy network are the determining factors for calculating the cost function.

$$w(t+1) = w(t) + K(t)e(t),$$
$$p(t+1) = p(t)\left[I - K(t)\varphi^T(t)\right], \tag{25}$$
$$K(t) = \frac{p(t)\varphi(t)}{R_n(t) + \varphi^T(t)p(t)\varphi(t)},$$

where the cost function is denoted by $(\partial E/\partial w)$ concerning the neurochaotic fuzzy network parameters and is computed using equation (26), in which the weights vector is represented by w in the previous subsections. Also, the derivative output of the neurochaotic fuzzy system in relation to the parameters of the rules is indicated by $\varphi(t)$. $(\partial E/\partial w)$ is calculated through equation (26), employing a chain derivative.

$$\frac{\partial E}{\partial w} = \frac{\partial E}{\partial \Delta f}\frac{\partial \Delta f}{\partial u_c}\frac{\partial u_c}{\partial \widehat{y}}\frac{\partial \widehat{y}}{\partial w}. \tag{26}$$

In accordance with equation (26), the control signal is u_c, and $\widehat{y}$ denotes the MLP neural network. Considering the neural system model, the system's Jacobian represented by $(\partial \Delta f/\partial u_c)$ is computed through the following equation:

$$E = \frac{1}{2},$$
$$e^2 = \frac{1}{2}(\Delta f)^2 \Rightarrow \frac{\partial E}{\partial \Delta f} = \Delta f,$$
$$u_c = \widehat{y} \Rightarrow \frac{\partial u_c}{\partial \widehat{y}} = 1, \tag{27}$$
$$\widehat{y} = w^T Z \Rightarrow \frac{\partial \widehat{y}}{\partial w} = Z.$$

The considered approach in the present research is shown in Figure 5 as a flowchart.

3.7. Structure of the Proposed Controller. The benefit of using an adaptive controller is its remarkable performance in tackling parametric and seismic uncertainties. Besides, a trade-off between stability and accuracy has a prominent role in the popularity of this type of controller. Many authors [121–129] have used smart systems for controlling, like fuzzy logic, artificial neural networks (ANNs), and or neural-fuzzy networks, to indicate complicated systems and create state-of-the-art controllers. The control strategies in the related studies were organized into two classes: (1) the system dynamics is known, and the controller is designed online. (2) The system dynamics is assumed to be unknown, and the controller is designed offline. Hence, evolutionary algorithms can be used to optimize the controllers, and optimized parameters are applied to the system. In fact, the system parameters are assumed to be implicitly known. The disadvantages of these methods are their time-consuming nature and the fact that they may not achieve an optimal operating point, which increases the computational work and may lead to control instability. Figure 6 outlines the proposed

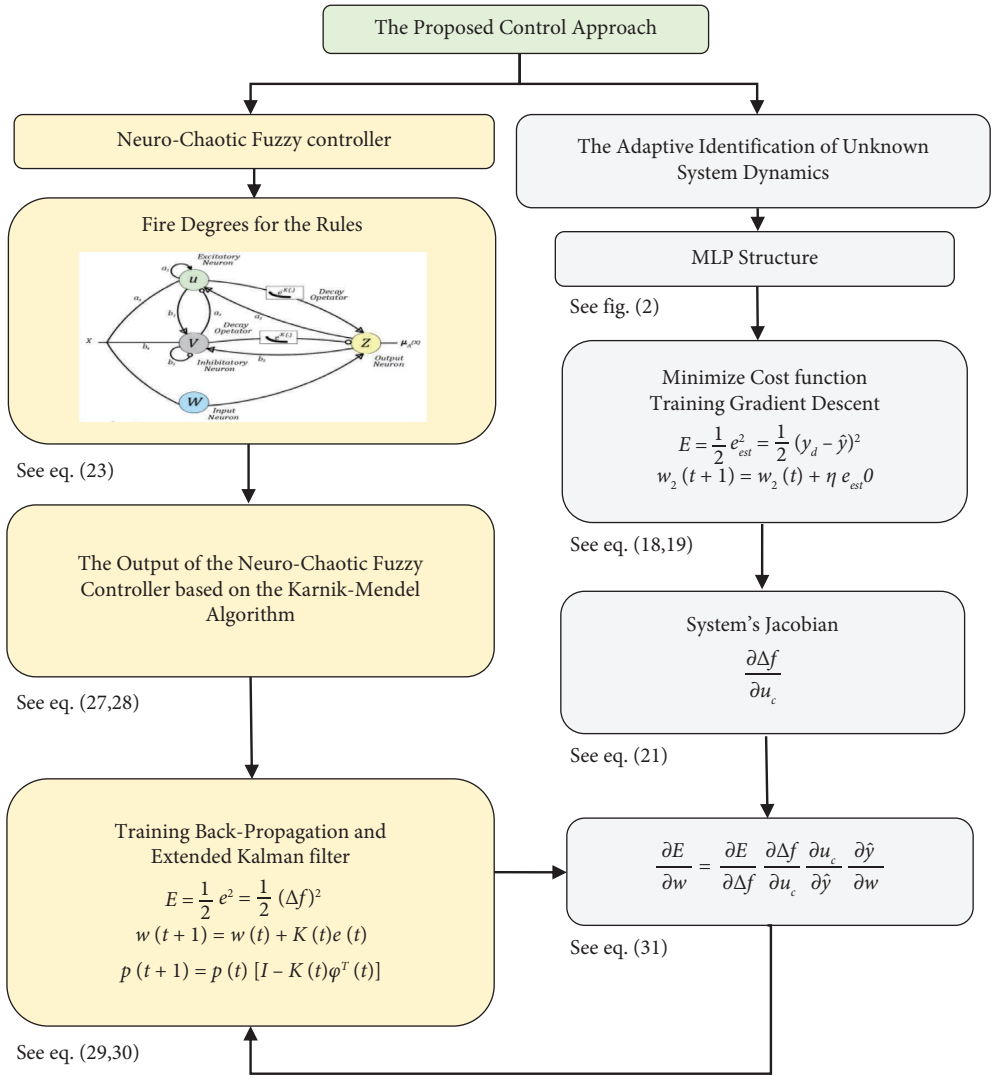

Figure 5: The flowchart of the proposed control strategy.

approach block diagram. The parameters of the system of this analysis are considered unknown and are estimated online by using the MLP neural network. The novel adaptive neurochaotic fuzzy controller (ANCF) is created online so that the system's output is online too. In this condition, the neurochaotic fuzzy network output is considered as the control signal. If the roof displacement is minimized, the control purpose is obtained.

The significant features of the proposed control system compared to the previous studies in this regard are as follows:

(i) There is no need to adjust the parameters of the adaptive neurochaotic fuzzy controller through the operator.

(ii) This controller can overcome uncertain parameters and a time-varying system.

(iii) A fractional-order proportional-integral-derivative (FOPID) has been added to the neurochaotic fuzzy controller to raise the proposed control strategy's stability and robustness.

(iv) The completely uncertain dynamics are considered in the structural system, and there is no need for the Jacobian of the plant.

3.8. Alternative Controller. In this paper, to evaluate the performance of the Type-2 neural-fuzzy controller, the simple adaptive control (SAC) controller is also considered. This model-based adaptive control algorithm was introduced by Sobel et al. in 1982 [79]. Since the SAC method is a direct adaptive method, it is used in complex systems with a high degree of freedom to maintain the performance of the controlled system under conditions of random loading and parametric uncertainties. In this algorithm, the behavior of the controlled system is compared with the behavior of an ideal reference model defined by the designer, and by applying appropriate control forces, the behavioral difference between them is reduced. Due to the simplicity of the structure, the ability to maintain efficiency under environmental uncertainties (dynamic loads of earthquakes and disturbances in sensors), independence from the

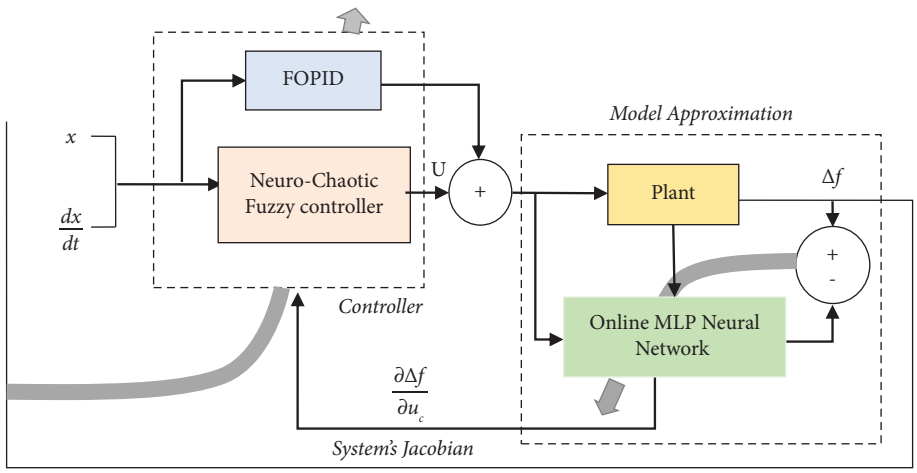

Figure 6: The structure of the proposed control system.

dynamic parameters of the controlled system (efficiency under the conditions of the damaged structure), and the freedom of the designer to select the type and order of the reference model (the possibility of using a model with a smaller order than the plant), the SAC algorithm is considered a suitable optimization technique in the active control of structures. Recent years have witnessed remarkable growth in the use of this algorithm for controlling structures [130]. Figure 7 shows the diagram block of this control method.

Considering equations (28) and (29), the dynamic behavior of the controlled structure (plant) is shown in the form of state space [131, 132].

$$\dot{x}_p(t) = A_p x_p(t) + B_p u_p(t) + d_p, \tag{28}$$

$$y_p(t) = C_p x_p(t) + d_0. \tag{29}$$

According to the equations above, x_p shows the state vector of plan $n \times 1$, the input control vector of $m \times 1$ is represented by u_p, and the output plant of $q \times 1$ is shown by y_p. Besides, the state matrix of $n \times n$ is shown through A_p, B_p indicates the input matrix of $n \times m$, and C_p shows the output matrix of $q \times n$. It should be noted that $d_p(t)$ and $d_0(t)$ indicate the disturbances applied to the system and the disturbances existing in the sensors, respectively [131, 133].

The aim here is to find the input control of $u_p(t)$ (without any information regarding the system parameters) for tracking the output of the ideal reference model by the system output. According to the state space, the reference model is indicated in the following equations [131]:

$$\begin{aligned} x_m(t) &= A_m x_m(t) + B_m u_m(t), \\ y_m(t) &= C_m x_m(t), \end{aligned} \tag{30}$$

where x_m shows the state vector of the reference model of $n_m \times 1$, u_m is the input control vector of $m \times 1$, and y_m shows the reference output vector of $q \times 1$. Also, A_m indicates the state matrix of $n_m \times n_m$, B_m denotes the input matrix of $n_m \times m$, and the output matrix of $q \times n_m$ is demonstrated by C_m [131, 133]. It should be noted that the order of reference model n_m can be less than the order of plant n. Actually, this value must be large enough to perform the desired command for creating the plant [131, 134]. Accordingly, the system behavior characterized by the designers is easily shown through the ideal model (reference) regardless of the prior information about the plant's system parameters [132]. The output tracking error (the error between the reference model output and the plant output), denoted by $\overline{e}_y$, is minimized (approaching zero asymptotically) via the SAC method. The control commands must be calculated based on the whole available data for the ideal model by considering the states and inputs of the model in a feedforward configuration [132, 135].

$$\begin{aligned} \overline{e}_y(t) &= y_m(t) - y_p(t), \\ u_p(t) &= \widetilde{K}_e(t)\overline{e}_y(t) + \widetilde{K}_x(t)x_m(t) + \widetilde{K}_u(t)u_m(t) \\ &= \widetilde{K}(t)\widetilde{r}(t), \end{aligned} \tag{31}$$

where

$$\begin{aligned} \overline{K}(t) &= \left[\widetilde{K}_e(t) \quad \widetilde{K}_x(t) \quad \widetilde{K}_u(t)\right], \\ \widetilde{r}(t)^T &= \left[\overline{e}_y(t) \quad x_m(t) \quad u_m(t)\right]^T. \end{aligned} \tag{32}$$

The term $\widetilde{K}_e(t)$ is considered for indicating the time-varying stabilizing control gain matrix. Only $\widetilde{K}_e(t)\overline{e}_y(t)$ needs the stability of the control system here. Basically, $\widetilde{K}_x(t)$ and $\widetilde{K}_u(t)$ are considered to show the time-varying feedforward control gains for achieving the zero output tracking error. Such control gains for ensuring the controlled system's stability and minimizing the tracking error to zero asymptotically are achieved using the SAC technique. Calculating the adaptive control gains, $\widetilde{K}(t)$ can be extracted when the form of integral and proportional terms are integrated [132, 135].

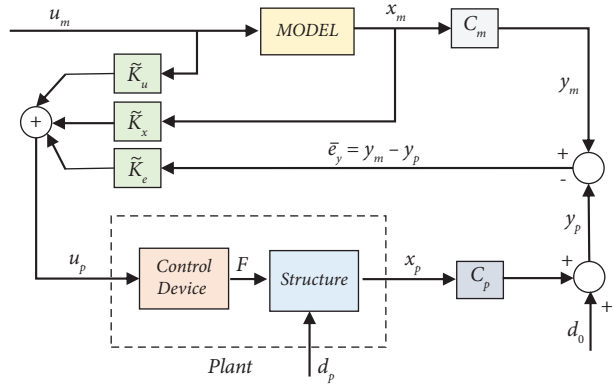

Figure 7: Block diagram of the simple adaptive control (SAC) system.

$$\tilde{K}(t) = \tilde{K}_I(t) + \tilde{K}_p(t), \tag{33}$$

where

$$\dot{\tilde{K}}_I(t) = \bar{e}_y(t)\tilde{r}(t)^T\hat{T} - \tilde{\sigma}\tilde{K}_I(t), \tag{34}$$

$$\tilde{K}_p(t) = \bar{e}_y(t)\tilde{r}(t)^T T, \tag{35}$$

where $\hat{T}$ is the diagonal positive-definite matrix, and this term defines the adaptation rate of the control gains. On the other hand, the constant coefficient matrix is shown by T. The proportional term $\tilde{K}_p(t)$ also indicates the immediate fine for large-scale errors. Using this term, the system is directed toward small-scale errors [131, 135]. Furthermore, in order to prevent integral gain divergence, $\tilde{\sigma}$ denotes the forgetting term matrix in equation (34) according to the disturbances that can be significantly small. When the $\tilde{\sigma}$ is not considered, $\tilde{K}_I$ is a full integrator, and this term constantly rises whenever total tracking ($\bar{e}_y = 0$) is not achievable. Consequently, this term might reach unnecessarily excessive values or even diverge [131].

As represented in equation (33) earlier, the integral adaptive control terms are considered for assuring stability in the direct adaptive method. The proportional adaptive control terms can be considered to increment the closed-loop system's convergence toward complete tracking [132, 135]. In order to adjust the SAC controller, the parameters of equations (34) and (35) must be regulated accurately. Trial and error are frequently used in the selection process for these parameters. Consequently, many sensitivity analyses are required, and it is unclear whether this results in the most suitable values or not [136, 137].

Regarding equation (36), the reference model is chosen at any time; the output y_m is confined to $-\tilde{Y}_{\max}$ and $\tilde{Y}_{\max}$ ($-\tilde{Y}_{\max} \le y_m \le \tilde{Y}_{\max}$) under unknown u_m inputs. It is assumed that any sensor does not measure the acceleration of the earthquake. Thus, the term $\tilde{K}_u(t)u_m(t)$ is excluded from the process of creating the control command. The following are the conditions of the reference model:

$$\begin{cases} x_m = \begin{bmatrix} \tilde{X}_m \\ \dot{\tilde{X}}_m \end{bmatrix} \\ = \begin{bmatrix} \int \dot{\tilde{X}}_m dt \\ \dot{\tilde{X}}_m \end{bmatrix} \\ = \begin{bmatrix} \int y_m dt \\ y_m \end{bmatrix}, \\ y_m = y_p, \qquad \text{if } |y_p| < \tilde{Y}_{\max}, \\ y_m = \text{sign}(y_p)\tilde{Y}_{\max}, \quad \text{if } |y_p| \ge \tilde{Y}_{\max}. \end{cases} \tag{36}$$

According to equation (36), $\tilde{X}_m$ and $\dot{\tilde{X}}_m$ show the displacement and velocity of the reference model, respectively. Also, $\tilde{Y}_{\max}$ is considered to show the maximum acceptable amount of the model output, which might be any value equivalent to or more than zero. The optimal value for $\tilde{Y}_{\max}$ is determined by the study's goal based on minimizing the drift, acceleration, or other structural responses. In the present study, $\tilde{Y}_{\max} = 0$, according to which the control is designed to reduce the displacement of the structure's top floor. As an innovation, the suitable values of the parameters of the matrix $\tilde{\sigma}$ and diagonal matrices $\hat{T}$ and T are tuned by employing PSO at any time. Therefore, an improved form of SAC, namely ISAC, is proposed in this research. The limitation of the ISAC controller method includes considering the maximum control force equal to 5% of the structure's weight. The PSO algorithm and its objective function are as follows.

This is a population-based optimization method, where the population is called a group. A group of N particles moving around a D-dimensional search space. In this case, in the algorithm, the position of the i-th particle in each group is defined as $x_i = (x_{i1}, x_{i2}, \ldots, x_{ij}, \ldots, x_{ik})$ and the speed for the i th particle of the algorithm can be as $v_i = (v_{i1}, v_{i2}, \ldots, v_{ij}, \ldots, v_{ik})$.

In general, the position and speed of each particle are in the range of $[-X_{\max}, X_{\max}]^D$ and $[-V_{\max}, V_{\max}]^D$. Each particle is searching for the optimal point and is moving; otherwise, it cannot search, and because of this displacement, it also has speed. In fact, each particle is simultaneously based on shared information. It evolves with its neighboring particles. This work causes particles to choose a suitable solution using memory and group knowledge.

Particle swarm optimization begins when a group of particles (solutions) are randomly generated and tries to find the optimal solution by updating the generations. In the initialization phase, the initial population of particles must be created. In the particle optimization algorithm, each particle represents a solution to the problem, and a solution here is the vehicle's route; in each step, each route is updated using the two best values. To be the first case is the best position that the particle has reached so far.

The said position is known as pbest. If we define the position of the particles as a set $p_i = (p_{i1}, p_{i2}, \ldots, p_{iD})$, the best position of the i-th particle is called pbest_i. If we define the value of the positions obtained by pbest_i of particles as a set $g_i = (g_1, g_2, \ldots, g_D)$. The best value of this set is gbest_i. PSO is initialized with a random particle population. Then the algorithm is executed by searching for optimal solutions and continuously updating the generation. In each generation, the position and velocity of the i-th particle are indicated by pbest_i and gbest_i and are updated using relations (37) and (38). In fact, the goal of the algorithm is to update particle position.

$$v_{\text{id}}^{\text{new}} = w \times v_{\text{id}}^{\text{old}} + c_1 \times r_1 \times \left(\text{pbest}_{\text{id}} - x_{\text{id}}^{\text{old}}\right) + c_2 + r_2 \times \left(\text{gbest}_d - x_{\text{id}}^{\text{old}}\right), \tag{37}$$

$$x_{\text{id}}^{\text{new}} = x_{\text{id}}^{\text{old}} + v_{\text{id}}^{\text{new}}. \tag{38}$$

In the above relations, r_1 and r_2 are random numbers in the interval (0, 1), c_1 and c_2 are acceleration constants that control how a particle moves in one generation. The speeds $v_{\text{id}}^{\text{new}}$ and $v_{\text{id}}^{\text{old}}$ represent the speed of new and old particles, respectively. $x_{\text{id}}^{\text{old}}$ shows the current position of the particle, and $x_{\text{id}}^{\text{new}}$ shows the updated position of the particle. w is the inertial weight that is defined to control the effect of the previous speed of particles in a flow, B is the number of iterations, and N is the number of particle populations. Therefore, in this article, the objective function is to minimize the displacement of the roof floor and the parameters of the algorithm PSO are selected as follows:

$$\begin{aligned} B &= 100, \\ N &= 20, \\ V_{\max} &= 2, \\ w &= 1, \\ c_1 &= c_1 = 2. \end{aligned} \tag{39}$$

4. Numerical Analysis

4.1. Structure Specifications and Dynamics. In this subsection, the major information regarding the 11-story structure considered for numerical analysis is given, and the benefits of the proposed control method are outlined. This building is located in Rasht. Each floor in this building has a rigid diaphragm, and all of the building mass is lumped at the floor levels. Also, a simplified linear model is adopted here. The structure used in this study has rigid beams and columns with axially rigid and flexible features to lateral deformation. Instead of the equivalent stiffness for the floors, spring stiffness is considered. A two-dimensional shear-type building model was selected to analyze the problem concerning the mentioned assumptions. The displacements of each floor are defined by a degree of freedom (DOF). The top floor has a TMD so that the total displacement of the floors plus TMD is shown by 12 degrees of freedom. Besides, the control system contains an ATMD on the highest floor of the structure. Table 1 illustrates the mass and stiffness values for each floor in this structure [43].

Employing a linear spring and a viscous damper, the TMD is modeled. Notably, the frequency ratio denoted by β_{TMD} is assumed to specify the ratio between the natural frequency of the TMD and the first modal frequency in the primary building. Besides, α_{TMD}-percent of the total mass is regarded as the TMD's mass, and ξ_{TMD}-percent of the critical damping value is allocated to the damping ratio of the TMD. Considering a genetic algorithm, α_{TMD}, ξ_{TMD}, and β_{TMD} have the optimal percentages of 3%, 7%, and 1.0, respectively. In the uncontrolled structure's initial and secondary natural frequencies, the values of $\omega_1 = 6.57$ and $\omega_2 = 19.36$ rad/s are calculated. Furthermore, the structural damping ratio value is equal to 5% of the critical damping value in the first two modes. The damping matrix is achieved using Rayleigh's method (equation (5)) [43]. Also, information regarding the Δ_M and Δ_K values is presented in Table 2.

4.2. Earthquake Site. Four known earthquakes were used to assess the performance of the proposed adaptive neuro-chaotic fuzzy controller on a structural system equipped with ATMD under the analysis of the time history of the structure using the MATLAB/Simulink software package [43, 138]. The International Association of Structural Control (IASC) has reported two far-fields (El Centro 1940 and Hachinohe 1968) and two near-fields (Northridge 1994 and Kobe 1995) ground acceleration records to investigate the performance of control systems for seismic applications. These earthquakes had an absolute peak ground acceleration (PGA) of 0.3417, 0.2250, 0.8267, and 0.8178 g, respectively (see Figure 8).

Table 1: The main parameters' values for the proposed building.

Story no.	Mass/ ($\times 10^3$kg)	Stiffness/ ($\times 10^6$N/m)
1	215	468
2	201	476
3	201	468
4	200	450
5	201	450
6	201	450
7	201	450
8	203	437
9	203	437
10	203	437
11	176	312

Table 2: The nominal and perturbed models with their uncertainty factors' values.

Models	Nominal model	Model (1)	Model (2)	Model (3)	Model (4)
Δ_M	0.00	+0.15	+0.15	−0.15	−0.15
Δ_K	0.00	+0.20	−0.20	+0.20	−0.20

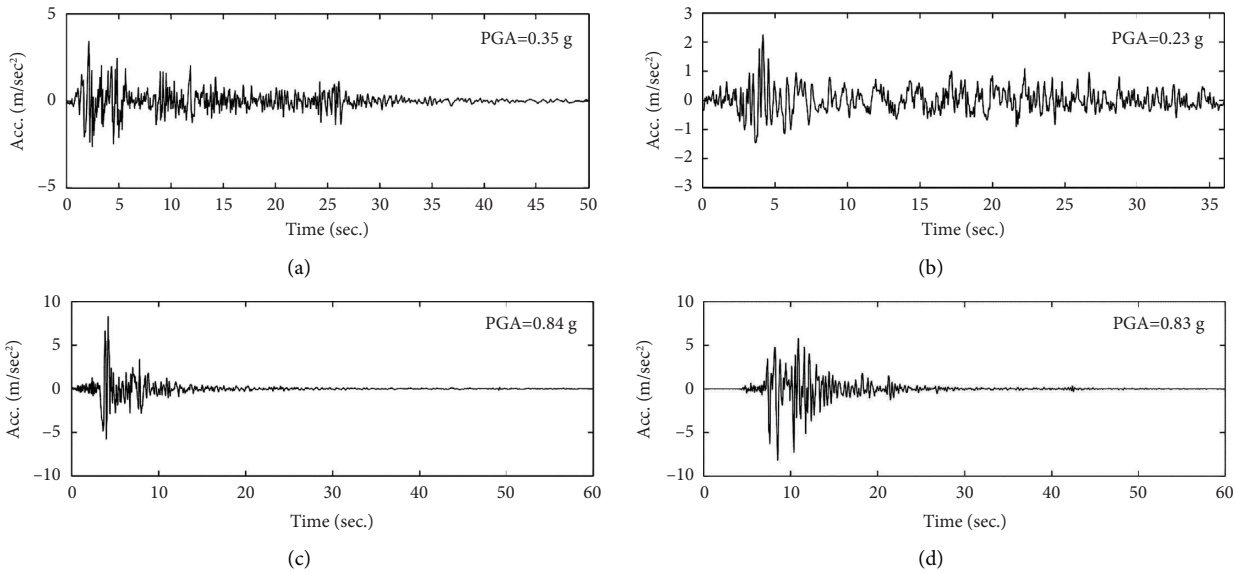

Figure 8: Time history of earthquake records considered. (a) El centro 1940. (b) Hachinohe 1968. (c) Northridge 1994. (d) Kobe 1995.

5. Results and Discussion

In order to prove the unique performance of the ANCF controller over the state-of-the-art ones, an assessment is made between the ANCF and ISAC controllers in terms of the main parameters, such as maximum displacement, acceleration, drift, base shear, and robustness against uncertainties. For this purpose, the 11-story building equipped with ATMD subjected to four well-known earthquakes is investigated by time history analysis.

5.1. Analytical Results. As regards Tables 3–6, the performance of the controllers is compared with the previous ones, respectively. Accordingly, these tables indicate the maximum displacement of stories under seismic excitations in the uncontrolled condition for the structure equipped TMD (passive) [43] and the controlled structure by LQR [43], FLC [43], OSMC [56], FOPID [61], OSAC [113], and AT2NF [113]. Overall, the ability of the proposed ISAC and ANCF controllers by far outperforms the other state-of-the-art control strategies, considering the maximum displacement reduction. Considering the top story, ISAC controller decreased 74%, 75.2%, 68.1%, and 66.8% based on the reported earthquakes. Interestingly, such values for the ANCF controller are 90%, 91.1%, 80.6%, and 84.1%, representing the superiority of the ANCF controller over the ISAC controller. The proposed controllers have better performance in far-field earthquakes than in near-field ones. Also, the lowest and highest reductions on average are related to the Northridge earthquake, controlled by TMD, with 6.5%, and the Hachinohe earthquake, controlled by ANCF controller, with 90.2%. The results represent the dependency of TMD

Table 3: The maximum displacements of stories in the El Centro earthquake.

Story	The highest values for the responses of floors (m)										The percentage of the reduction (%)								
	Unctrl. [43]	Passive [43]	LQR [43]	FLC [43]	OSMC [56]	FOPID [61]	OSAC [113]	AT2NF [113]	ISAC	ANCF	Passive [43]	LQR [43]	FLC [43]	OSMC [56]	FOPID [61]	OSAC [113]	AT2NF [113]	ISAC	ANCF
1	0.019	0.013	0.009	0.090	0.008	0.009	0.005	0.003	0.006	0.002	31.6	52.6	52.6	57.9	52.6	73.2	85.5	70.5	88.0
2	0.039	0.025	0.018	0.016	0.016	0.016	0.010	0.005	0.011	0.004	35.9	53.8	59.0	59.0	59.0	74.9	86.5	72.4	88.6
3	0.057	0.037	0.027	0.023	0.024	0.023	0.014	0.008	0.016	0.006	35.1	52.6	59.6	57.9	59.6	74.9	86.4	72.4	88.6
4	0.074	0.048	0.035	0.028	0.032	0.029	0.019	0.010	0.021	0.008	35.1	52.7	62.2	56.8	60.8	74.7	86.4	72.1	88.6
5	0.090	0.058	0.043	0.034	0.041	0.034	0.023	0.012	0.025	0.010	35.6	52.2	62.2	54.4	62.2	74.6	86.5	72.1	88.6
6	0.100	0.067	0.050	0.039	0.047	0.038	0.026	0.014	0.029	0.012	34.4	51.0	61.8	53.0	62.8	73.5	86.0	70.9	88.2
7	0.120	0.074	0.058	0.043	0.053	0.041	0.030	0.016	0.033	0.013	38.3	51.7	64.2	55.8	65.8	75.4	87.1	72.9	89.1
8	0.130	0.083	0.060	0.047	0.058	0.043	0.032	0.017	0.035	0.014	36.2	53.9	63.9	55.4	66.9	75.3	87.1	72.8	89.2
9	0.140	0.094	0.067	0.049	0.062	0.044	0.034	0.018	0.037	0.015	32.9	52.1	65.5	55.7	68.6	75.8	87.3	73.4	89.5
10	0.140	0.094	0.070	0.050	0.064	0.046	0.035	0.018	0.038	0.015	32.9	50.0	64.3	54.3	67.1	75.1	86.9	72.6	89.3
11	0.147	0.099	0.072	0.051	0.065	0.049	0.035	0.019	0.038	0.015	32.7	51.0	65.3	55.8	66.7	76.3	87.3	74.0	90.0
Average	0.096	0.063	0.046	0.035	0.043	0.034	0.024	0.0014	0.026	0.0105	34.6	52.1	61.8	56.0	62.9	74.9	86.6	72.4	88.9

Table 4: The maximum displacements of stories in the Hachinohe earthquake.

Story	The highest values for the responses of floors (m)										The percentage of the reduction (%)								
	Unctrl. [43]	Passive [43]	LQR [43]	FLC [43]	OSMC [56]	FOPID [61]	OSAC [113]	AT2NF [113]	ISAC	ANCF	Passive [43]	LQR [43]	FLC [43]	OSMC [56]	FOPID [61]	OSAC [113]	AT2NF [113]	ISAC	ANCF
1	0.014	0.012	0.011	0.008	0.011	0.007	0.004	0.002	0.004	0.0016	14.3	21.4	42.9	21.4	50.0	73.1	83.6	74.9	88.6
2	0.028	0.024	0.021	0.017	0.021	0.005	0.007	0.004	0.007	0.0031	14.3	25.0	39.3	25.0	82.1	73.9	84.3	75.6	88.9
3	0.040	0.035	0.032	0.024	0.030	0.005	0.011	0.006	0.010	0.0043	12.5	20.0	40.0	25.0	87.5	73.0	84.3	74.8	89.3
4	0.053	0.046	0.041	0.030	0.039	0.005	0.014	0.008	0.013	0.0054	13.2	22.6	43.4	26.4	90.6	73.2	85.0	75.0	89.8
5	0.064	0.055	0.050	0.036	0.047	0.051	0.018	0.009	0.016	0.0063	14.1	21.9	43.8	26.6	20.3	72.6	85.4	74.4	90.2
6	0.074	0.064	0.058	0.040	0.052	0.050	0.021	0.011	0.019	0.0069	13.5	21.6	45.9	29.7	32.4	72.1	85.8	73.9	90.7
7	0.085	0.073	0.065	0.046	0.057	0.047	0.024	0.012	0.022	0.0078	14.1	23.5	45.9	32.9	44.7	72.2	86.4	74.1	90.8
8	0.094	0.081	0.071	0.050	0.062	0.042	0.026	0.013	0.024	0.0087	13.8	24.5	46.8	34.0	55.3	72.2	86.6	74.1	90.7
9	0.100	0.089	0.076	0.053	0.066	0.046	0.028	0.014	0.026	0.0094	11.0	24.0	47.0	34.0	54.0	72.0	86.4	73.9	90.6
10	0.110	0.095	0.079	0.055	0.068	0.050	0.029	0.014	0.027	0.0097	13.6	28.2	50.0	38.2	54.5	73.6	86.9	75.4	91.2
11	0.110	0.099	0.083	0.057	0.070	0.051	0.029	0.015	0.027	0.0098	10.0	24.5	48.2	36.4	53.6	73.4	86.4	75.2	91.1
Average	0.070	0.061	0.053	0.038	0.048	0.033	0.019	0.010	0.018	0.007	13.1	23.4	44.8	30	56.8	72.8	85.6	74.7	90.2

Table 5: The maximum displacements of stories in the Kobe earthquake.

Story	The highest values for the responses of floors (m)										The percentage of the reduction (%)								
	Unctrl. [43]	Passive [43]	LQR [43]	FLC [43]	OSMC [56]	FOPID [61]	OSAC [113]	AT2NF [113]	ISAC	ANCF	Passive [43]	LQR [43]	FLC [43]	OSMC [56]	FOPID [61]	OSAC [113]	AT2NF [113]	ISAC	ANCF
1	0.060	0.049	0.050	0.046	0.037	0.038	0.019	0.012	0.020	0.010	18.3	16.7	23.3	38.3	37.5	68.5	79.8	66.4	79.8
2	0.120	0.098	0.101	0.092	0.057	0.075	0.037	0.024	0.040	0.019	18.3	15.8	23.3	37.5	37.5	68.8	80.0	66.7	80.0
3	0.180	0.149	0.144	0.131	0.113	0.106	0.056	0.036	0.060	0.029	17.2	20.0	27.2	37.2	41.0	69.0	80.0	66.9	80.0
4	0.240	0.199	0.192	0.180	0.151	0.141	0.074	0.048	0.079	0.038	17.1	20.0	25.0	37.1	41.4	69.1	80.1	67.0	80.1
5	0.290	0.238	0.241	0.229	0.186	0.169	0.091	0.059	0.098	0.047	17.9	16.9	21.0	35.9	41.8	68.5	79.7	66.4	79.7
6	0.340	0.289	0.269	0.258	0.219	0.191	0.107	0.069	0.114	0.055	15.0	20.9	24.1	35.6	43.9	68.5	79.7	66.4	79.7
7	0.390	0.332	0.308	0.293	0.248	0.209	0.121	0.078	0.129	0.062	14.9	21.0	24.9	36.4	46.3	69.0	80.0	67.0	80.0
8	0.430	0.361	0.344	0.335	0.273	0.225	0.132	0.086	0.141	0.068	16.0	20.0	22.1	36.5	47.7	69.2	80.1	67.2	80.1
9	0.460	0.391	0.363	0.354	0.293	0.238	0.141	0.091	0.150	0.072	15.0	21.1	23.0	36.3	48.4	69.3	80.2	67.3	80.2
10	0.480	0.408	0.374	0.360	0.306	0.250	0.147	0.095	0.156	0.075	15.0	22.1	25.0	36.3	47.9	69.5	80.2	67.4	80.2
11	0.500	0.420	0.390	0.370	0.315	0.256	0.149	0.097	0.159	0.076	16.0	22.0	26.0	37.0	48.8	70.1	80.6	68.1	80.6
Average	0.317	0.267	0.252	0.241	0.201	0.173	0.098	0.063	0.104	0.050	16.4	19.7	24.1	36.7	43.8	69.0	80.0	67.0	84.1

Table 6: The maximum displacements of stories in the Northridge earthquake.

Story	The highest values for the responses of floors (m)										The percentage of the reduction (%)								
	Unctrl. [43]	Passive [43]	LQR [43]	FLC [43]	OSMC [56]	FOPID [61]	OSAC [113]	AT2NF [113]	ISAC	ANCF	Passive [43]	LQR [43]	FLC [43]	OSMC [56]	FOPID [61]	OSAC [113]	AT2NF [113]	ISAC	ANCF
1	0.046	0.040	0.033	0.031	0.032	0.026	0.010	0.005	0.011	0.005	13.0	28.3	32.6	30.4	43.7	77.7	88.1	75.8	88.2
2	0.088	0.080	0.063	0.058	0.059	0.049	0.020	0.011	0.022	0.011	9.1	28.4	34.1	33.0	44.8	77.4	87.9	75.4	88.0
3	0.123	0.109	0.109	0.080	0.083	0.068	0.029	0.015	0.032	0.015	11.4	11.4	35.0	32.5	44.7	76.3	87.5	74.3	87.5
4	0.150	0.140	0.110	0.099	0.103	0.091	0.038	0.020	0.041	0.020	6.7	26.7	34.0	31.3	39.5	74.7	86.9	72.5	86.6
5	0.180	0.160	0.130	0.119	0.119	0.110	0.046	0.024	0.050	0.024	11.1	27.8	33.9	33.9	38.8	74.5	86.8	72.3	86.5
6	0.194	0.178	0.149	0.130	0.138	0.126	0.053	0.027	0.058	0.028	8.2	23.2	33.0	28.9	34.9	72.7	85.8	70.4	85.6
7	0.204	0.190	0.169	0.139	0.155	0.139	0.059	0.030	0.064	0.031	6.9	17.2	31.9	24.0	31.7	71.2	85.0	68.7	84.9
8	0.210	0.200	0.181	0.143	0.169	0.152	0.063	0.033	0.069	0.033	4.8	13.8	31.9	19.5	27.5	69.8	84.3	67.2	84.2
9	0.220	0.220	0.189	0.156	0.188	0.162	0.067	0.034	0.073	0.035	0.0	14.1	29.1	14.5	26.4	69.6	84.3	67.0	84.1
10	0.230	0.230	0.209	0.168	0.204	0.172	0.069	0.035	0.075	0.036	0.0	9.1	27.0	11.3	25.3	70.0	84.7	67.4	84.3
11	0.230	0.230	0.219	0.170	0.218	0.181	0.070	0.035	0.076	0.036	0.0	4.8	26.1	5.2	21.1	69.4	84.7	66.8	84.1
Average	0.170	0.162	0.142	0.118	0.133	0.116	0.048	0.025	0.052	0.025	6.5	18.6	31.7	24.1	34.4	73.0	86.0	70.7	85.8

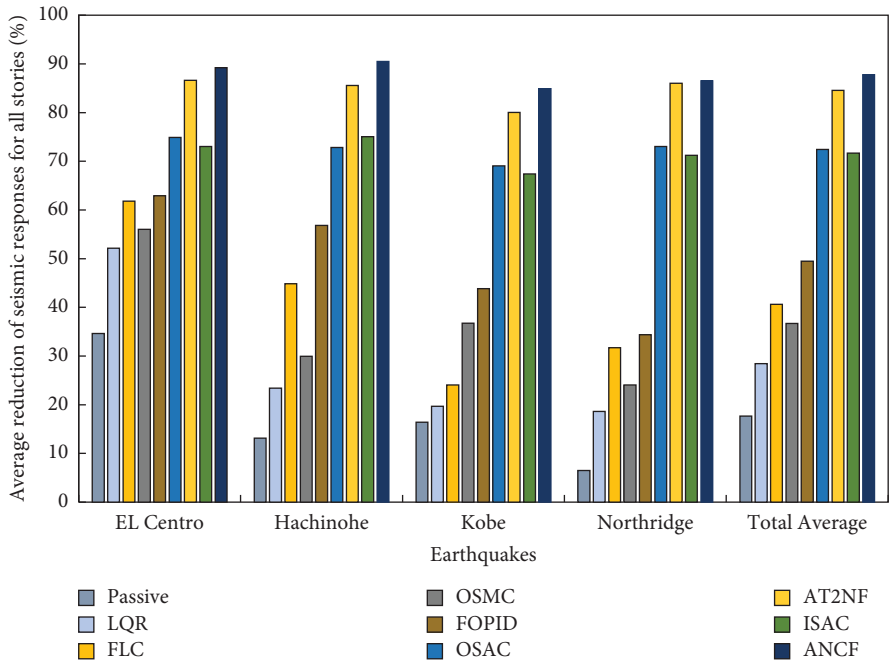

Figure 9: The average reduction of maximum structural responses for all stories.

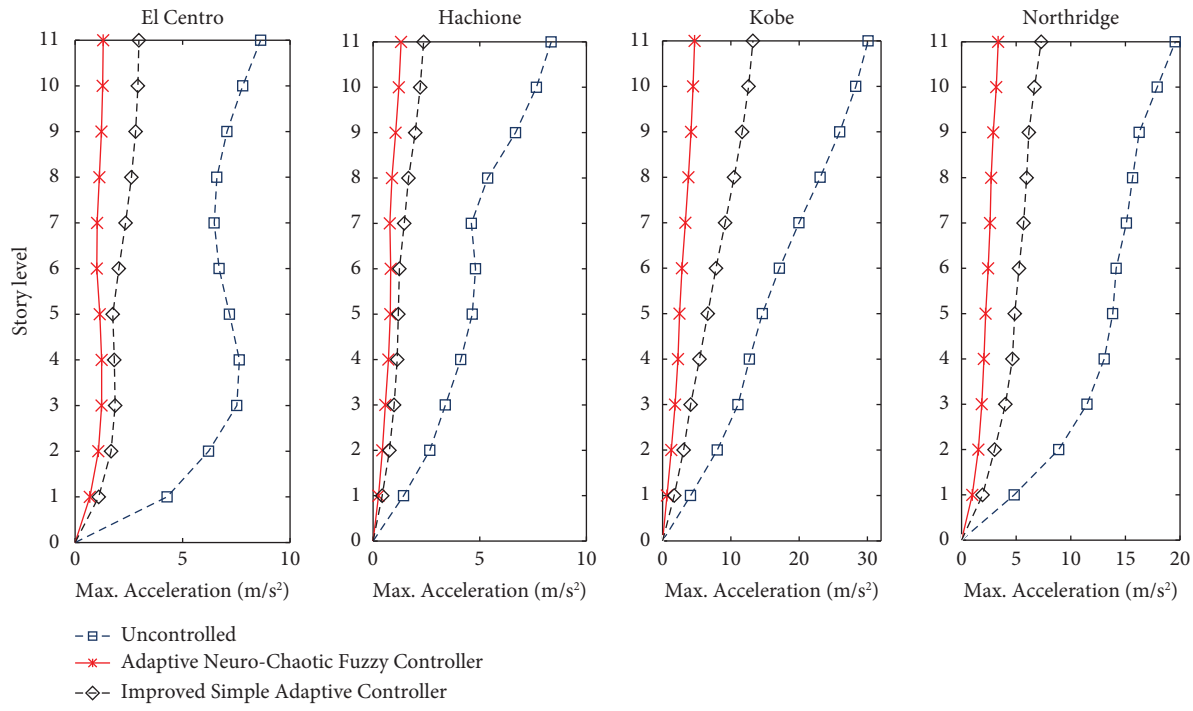

Figure 10: Maximum acceleration of the proposed controllers in all floors.

on the seismic inputs. It should be noted that the FOPID controller's performance with the top story's maximum displacement reductions of 66.7%, 53.6%, 48.8%, and 21.1% exposed to the considered earthquakes compete with the performance of LQR, FLC, and OSMC controllers. Additionally, the OSMC, FLC, and LQR compete in terms of efficiency. Comparing the results with the previous studies shows that ISAC and OSAC controllers almost have the same performance in terms of percentage of reduction, while the ANCF controller presents better results than the AT2NF controller so that the average percentage of displacement reduction in the ANCF controller under the El Centro earthquake is 88.9, which is about 3% better than the AT2NF controller; this percentage improvement decrease under the Hachinohe and Kobe earthquakes is about 5.5 and 5, respectively.

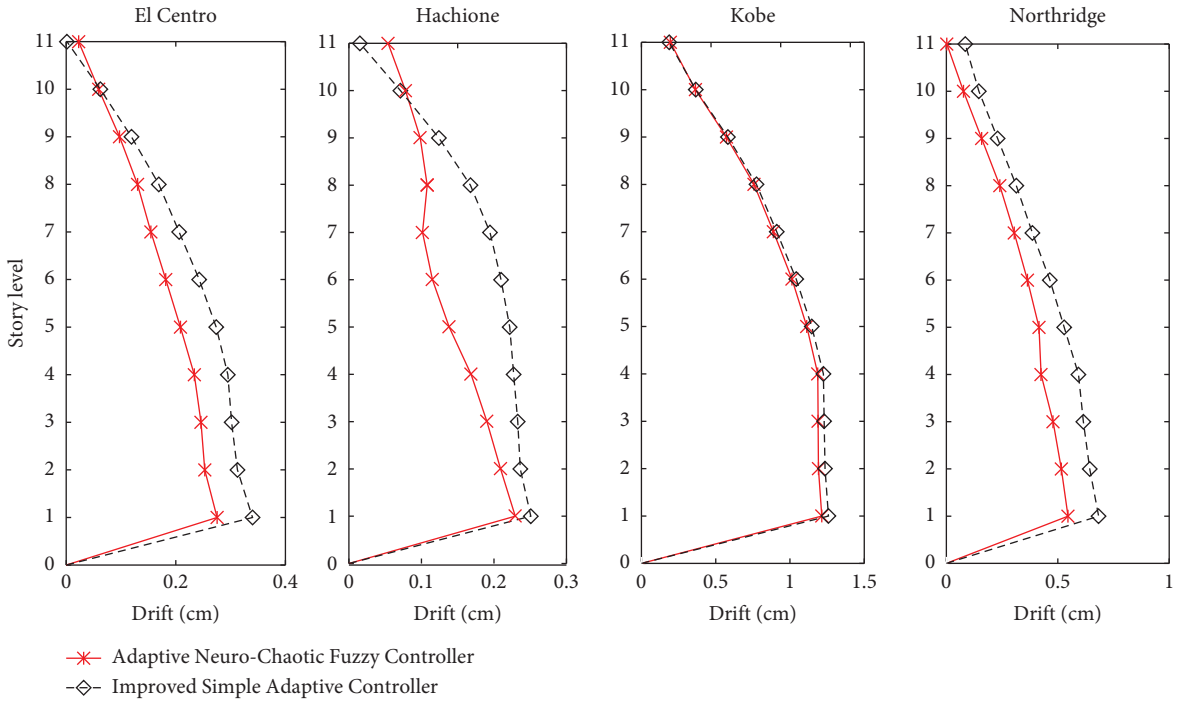

Figure 11: The drift of the proposed controllers ANCF and ISAC.

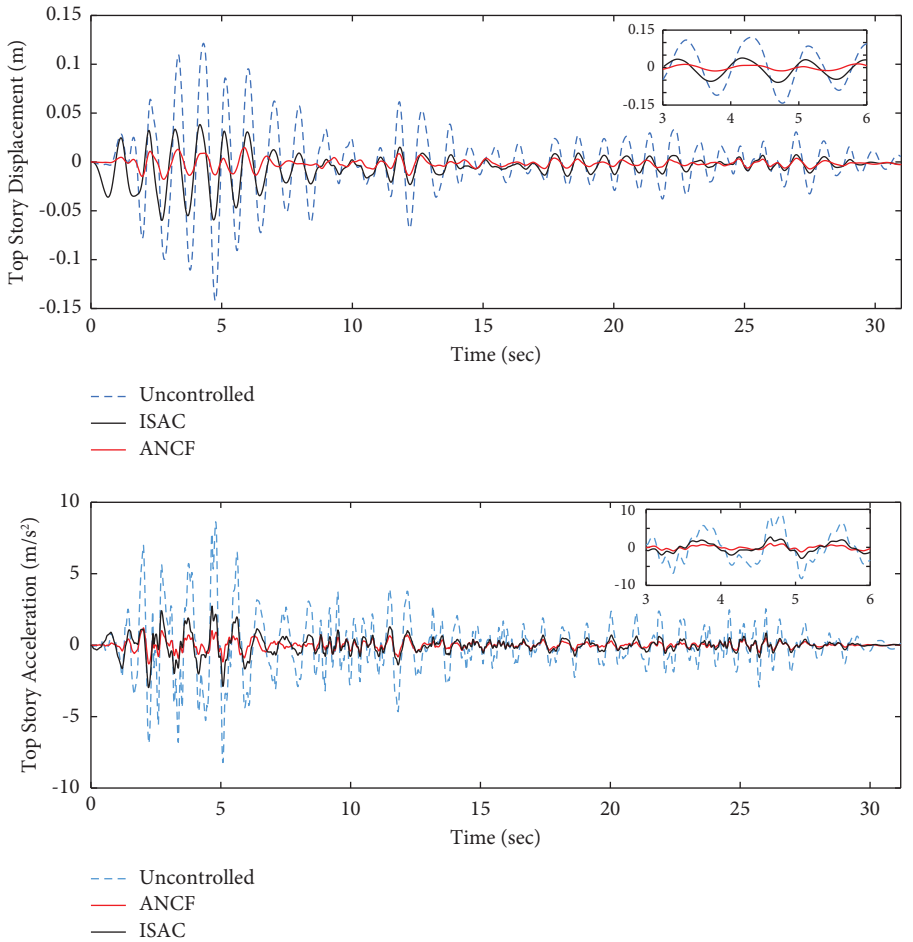

Figure 12: Time history of displacement and acceleration in the top story under the El Centro earthquake.

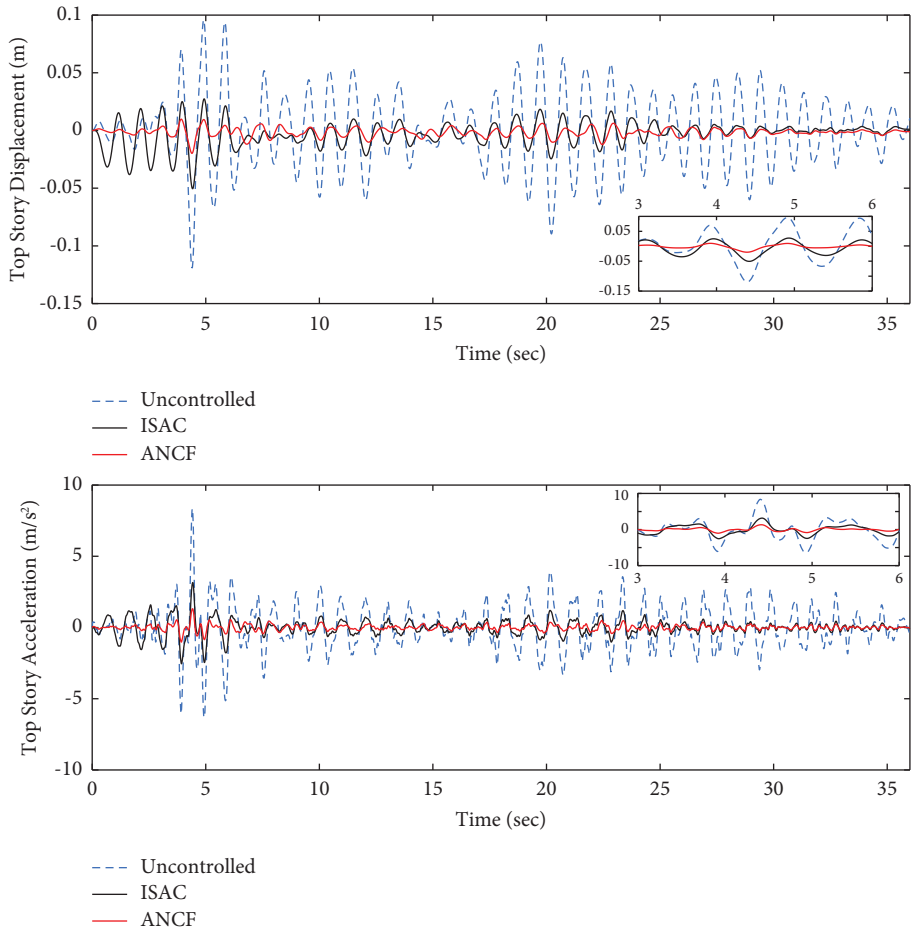

Figure 13: Time history of displacement and acceleration in the top story under the Hachinohe earthquake.

It is noteworthy that the root means squared (RMS) values of 3.01, 1.60, and 0.51 cm are attributed to the displacement of the highest floor subjected to the El Centro earthquake for the uncontrolled, ISAC, and ANCF controllers, which represents 46.9% and 83% reduction for ISAC and ANCF controllers. Besides, the ISAC controller gives the RMS values of 44.5%, 64.6%, and 58.6% reduction under the Hachinohe, Kobe, and Northridge earthquakes. Such values are 87.5%, 85.4%, and 82.0% for the ANCF controller.

All these highlight the better performance of the ANCF controller over the ISAC controller in terms of minimizing the structure's response. On the other hand, considering the seismic excitations, the highest limit of the allowable control force, which is typically 5% of the whole weight of the structure, is demanded by ISAC and ANCF controllers. As mentioned earlier, the control algorithm directly affects the tuning process of the control force. Due to the fact that the ANCF controller is not related to the structural parameters and is highly beneficial for identification, it successfully estimates the vibrations' intensification concerning the structure condition in which that applies the control force. Such advantages are highlighted by the superior performance of the ANCF controller, which is preferred to ISAC.

Moreover, considering the mentioned seismic excitations, Figure 9 compares the total average reduction of maximum structural responses between the state-of-the-art controllers, TMD, and adaptive ones proposed here. Clearly, the TMD performance is only acceptable in the limited range of load disturbances. Overall, the ANFC and ISAC controllers have delivered substantially better performance than the rest. However, the ANCF controller shows superiority with a total average reduction of 87.3%, about 16% more than the ISAC controller.

Regarding the maximum acceleration in the floor, the performance of the uncontrolled structure compared to the structure controlled with ANCF and ISAC controller is assessed in Figure 10. For example, the maximum acceleration reduction of 56% and 84.4% is obtained for ISAC and ANCF controllers under the Kobe earthquake. Overall, the ANCF and ISAC controllers indicate an average acceleration reduction of 84.1% and 64% for all earthquakes. Hence, the ANCF controller performed more successfully in this regard.

Figure 11 shows the drift (the difference between the displacement of the upper and lower floors) of the proposed ANCF and ISAC controllers, which indicates the superiority of the ANCF controller in reducing the drift compared to the ISAC controller.

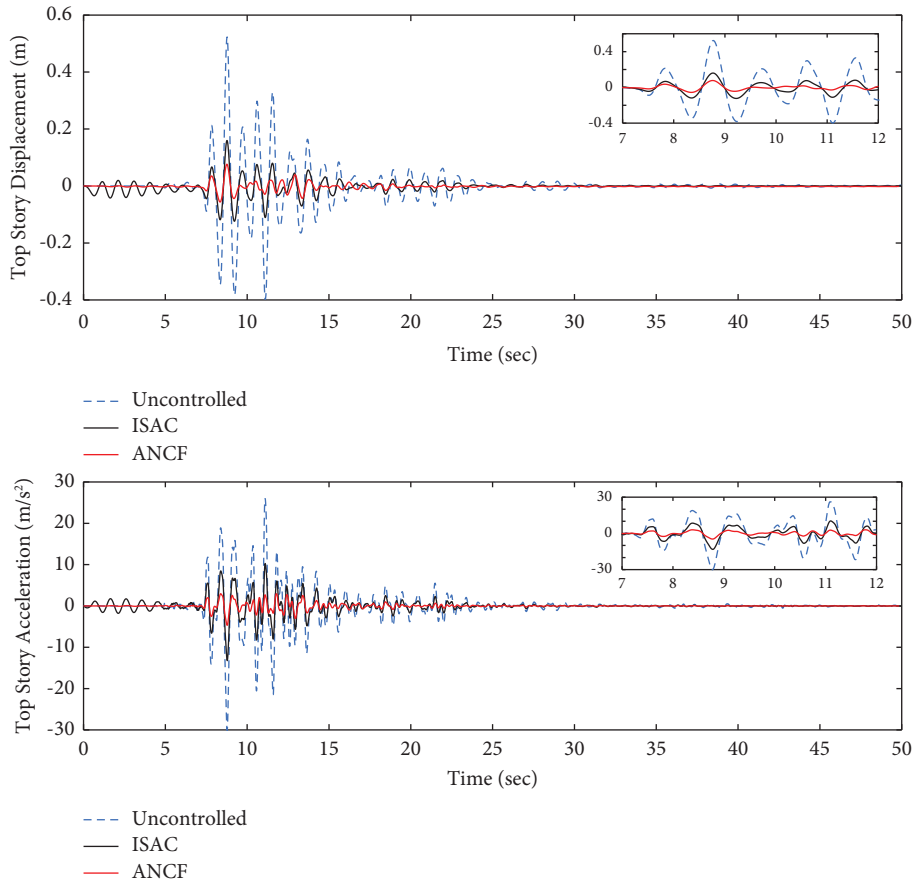

Figure 14: Time history of displacement and acceleration in the top story under the Kobe earthquake.

Furthermore, Figures 12–15 show the various time histories of the top story displacement and acceleration under the ISAC and ANCF controllers. According to the report on El Centro, Hachinohe, Kobe, and Northridge earthquakes and the obtained results, the ANCF controller performs better than the ISAC controller in reducing the maximum displacement and acceleration of floors.

In addition to the maximum displacement and acceleration, the proposed controllers' performance is compared in terms of base shear. For instance, according to Figure 16, the maximum responses in base shear under the El Centro earthquake are about 12700 KN, 8212 KN, and 3361 KN for uncontrolled conditions, ISAC, and ANCF controllers, respectively, which represent about 35.3% and 73.5% reduction for ISAC and ANCF controllers. In other words, the ANCF controller offers more base shear reduction of approximately 38% than the ISAC.

5.2. Validation Based on the Uncertainties. In this subsection, the performance of the proposed controller under uncertainties is examined to prove its validity. For this purpose, the initial stiffness matrix with −15% uncertainty is given as a perturbation (see Figure 17).

The maximum displacement response of the structure's top floor under the nominal and the perturbed models has been compared for both proposed adaptive controllers. The ACNF and ISAC controllers have been able to overcome the uncertainty in the stiffness of the structural system and effectively reduce the maximum displacement response of the structure's top floor. Accordingly, the percentage of deviation in the maximum displacement response of the structure's top floor compared to the nominal model of 9.2%, 10.4%, 13.2%, and 11.8% are observed when the structure was subjected to the El Centro, Hachinohe, Kobe, and Northridge earthquakes, respectively, and are controlled through the ISAC controller. However, the ACNF controller performs better than its counterpart here as the percentage of deviation in the maximum displacement response of the structure's top floor compared to the nominal model is 4.7%, 5.1%, 7.9%, and 6.9%, respectively. Finally, the maximum displacement values of the structure's top floor for ACNF and ISAC controllers under different uncertainties are compared, as shown in Figure 18. Regarding Table 2, the control system will likely lose its acceptable performance under the parametric variations. Hence, the proposed controllers' robustness against such variations is assessed here. The obtained results reveal that the ISAC controller is more susceptible to parametric changes than the ACNF controller. Notably, the ACNF controller performs well and significantly outperforms the ISAC controller in tackling parametric uncertainties. For instance, in model 2, the percentage of deviation in the maximum displacement response of the top floor of the structure compared to the

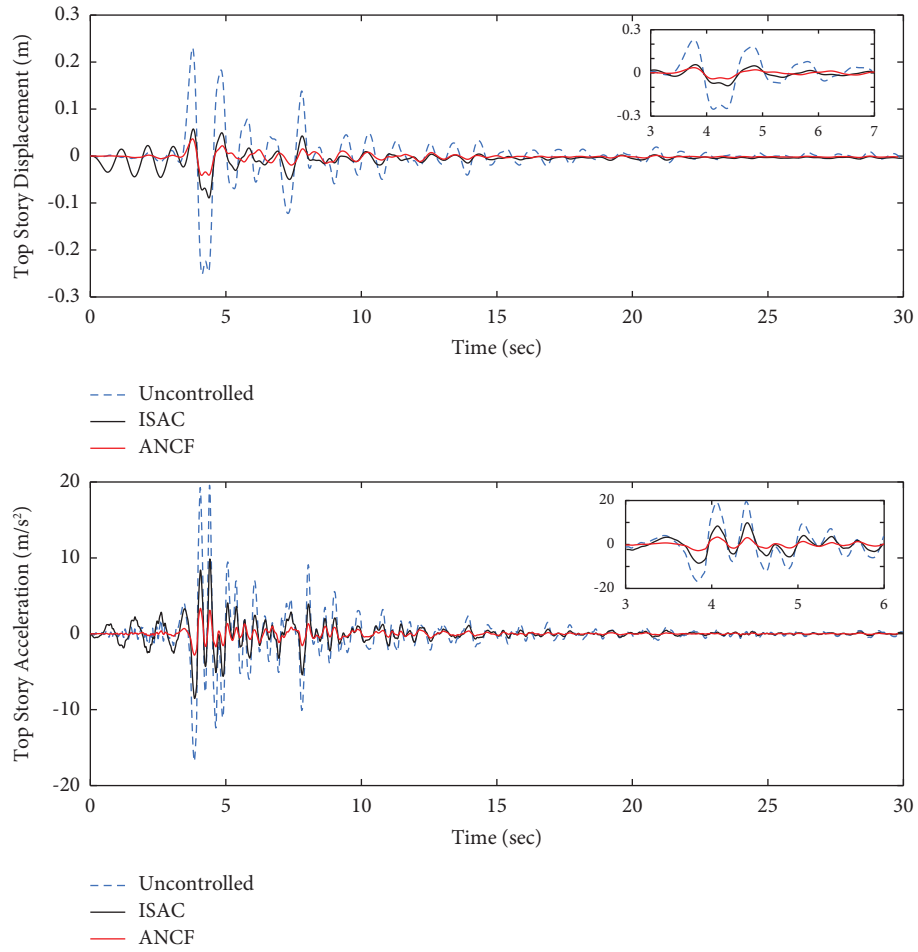

Figure 15: Time history of displacement and acceleration in the top story under the Northridge earthquake.

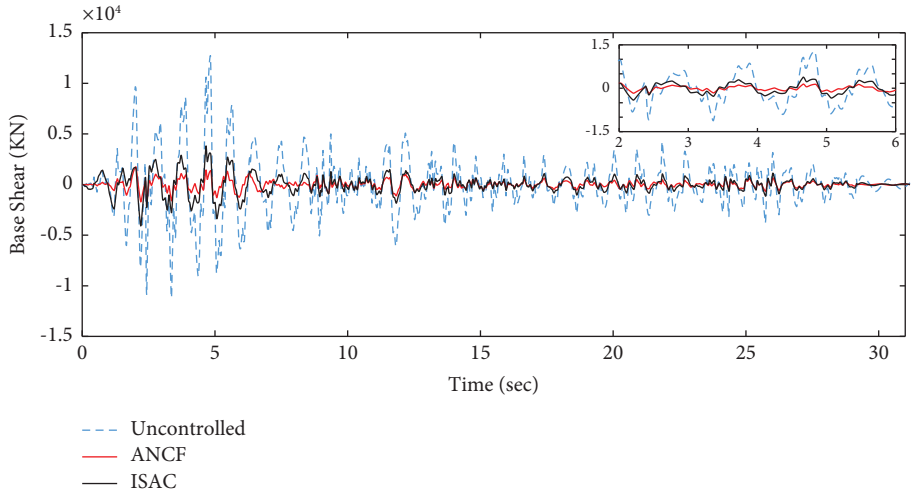

(a)

Figure 16: Continued.

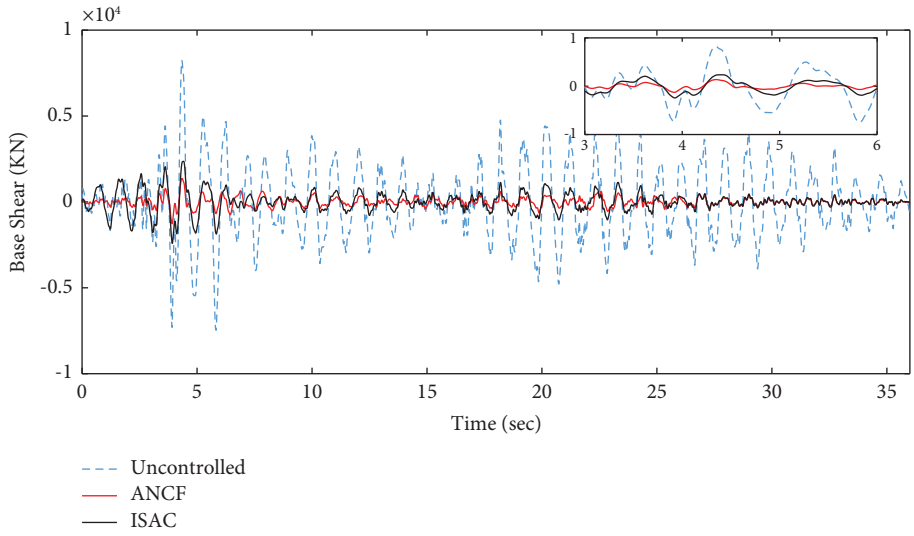

(b)

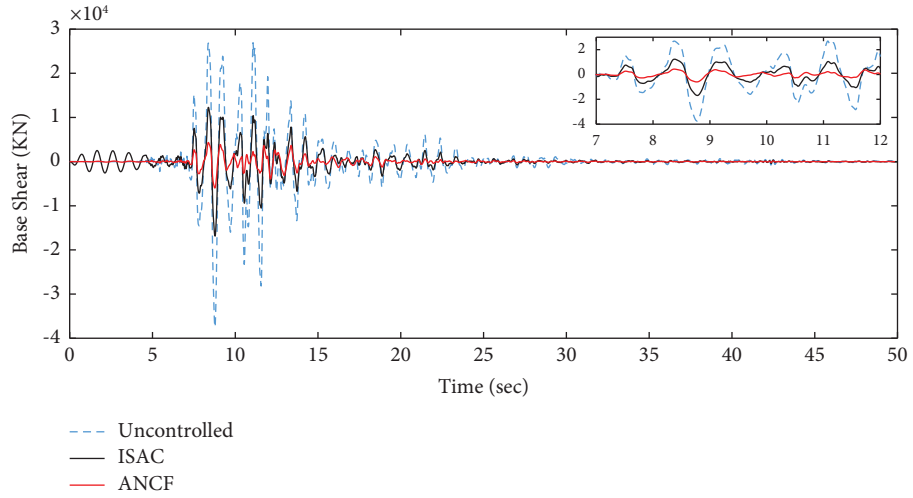

(c)

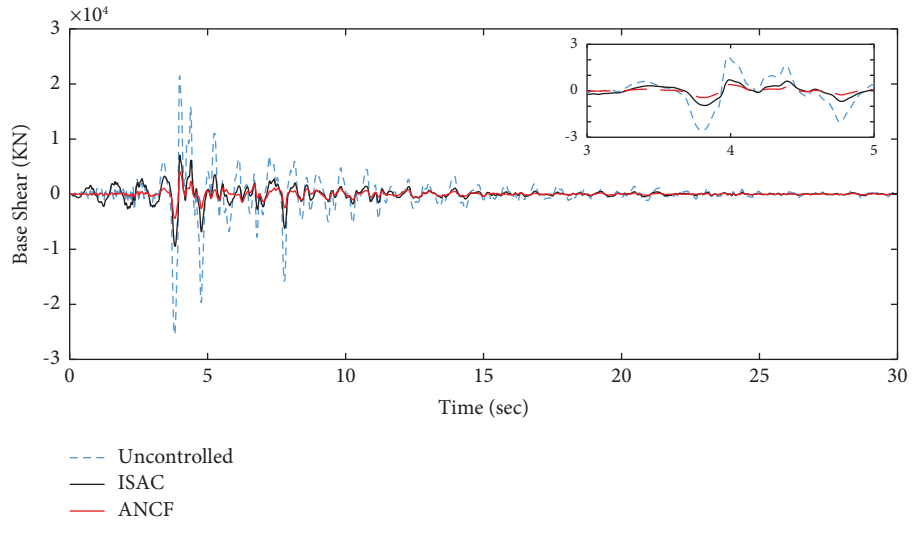

(d)

Figure 16: Time history of base shear under (a) the El Centro, (b) Hachinohe, (c) Kobe, and (d) Northridge earthquakes.

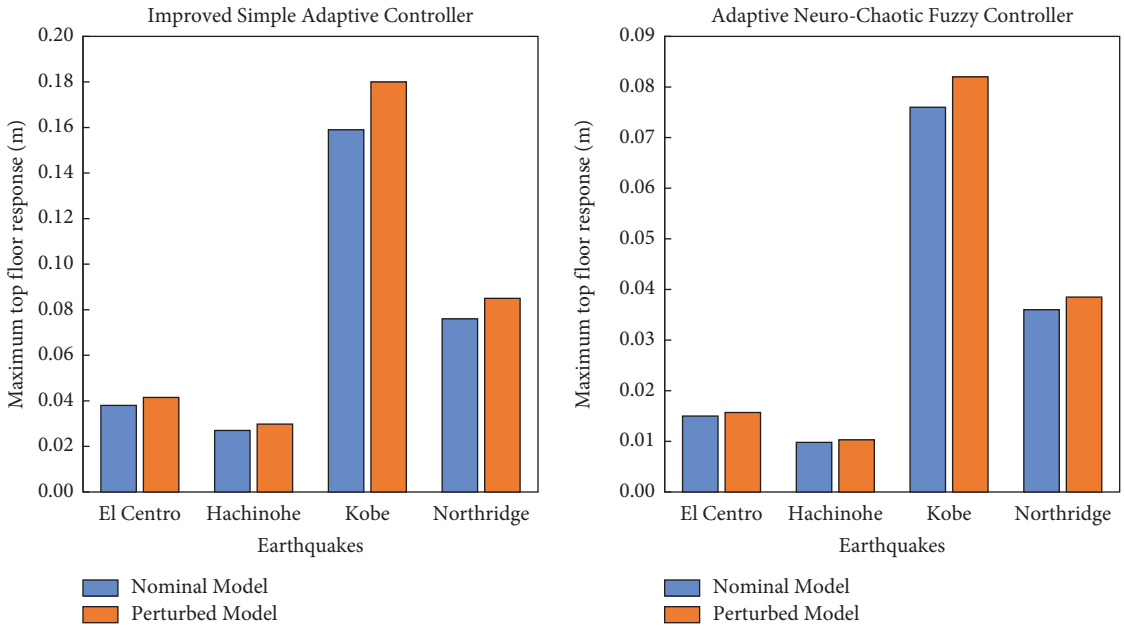

Figure 17: The maximum response values of the top floor in the nominal and perturbed model based on the proposed controllers.

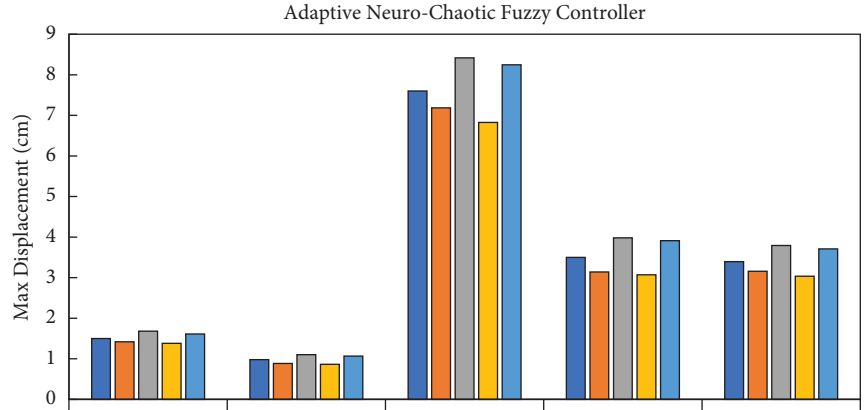

	El Centro	Hachinohe	Kobe	Northridge	Total Average
Nominal Model	1.50	0.98	7.60	3.50	3.40
Model 1	1.42	0.88	7.18	3.14	3.16
Model 2	1.68	1.10	8.42	3.98	3.79
Model 3	1.38	0.86	6.83	3.07	3.04
Model 4	1.61	1.07	8.25	3.91	3.71

(a)

Figure 18: Continued.

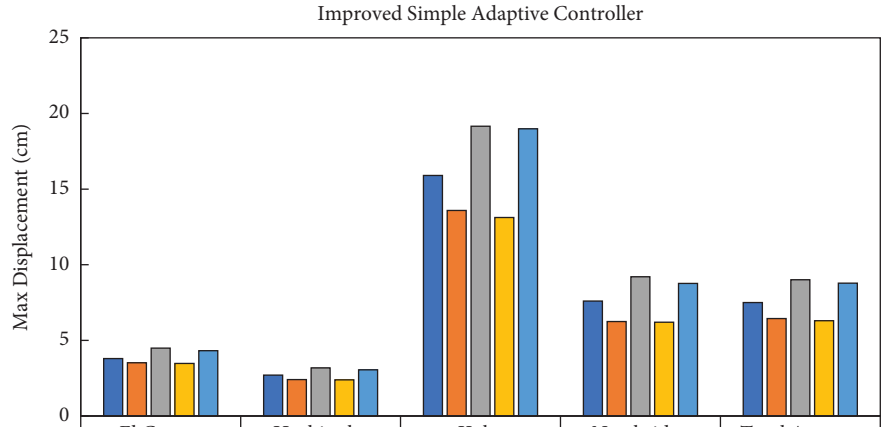

	El Centro	Hachinohe	Kobe	Northridge	Total Average
Nominal Model	3.80	2.70	15.90	7.60	7.50
Model 1	3.52	2.41	13.59	6.24	6.44
Model 2	4.49	3.18	19.16	9.20	9.01
Model 3	3.48	2.39	13.12	6.20	6.30
Model 4	4.32	3.05	18.98	8.77	8.78

(b)

Figure 18: The performance of (a) the ACNF controller and (b) the ISAC controller considering maximum displacement values of the top floor of the structure under various uncertainties.

nominal model in the ACNF controller are observed at 12%, 12.5%, 10.7%, 13.7%, and 11.7% under El Centro, Hachinohe, Kobe, and Northridge earthquakes, respectively. Such values for the controller of the ISAC controller are 18.2%, 17.6%, 20.5%, and 20.1%. Notably, a total average deviation for models 1–4 is 7%, 11.8%, 10.6%, and 9.2% relative to the ACNF controller, while these values for the ISAC controller are 14.2%, 20.1%, 16%, and 17% under the same seismic excitations.

6. Conclusion

This paper presents two new adaptive controllers with unique performance, ACNF and ISAC controllers, which have significantly reduced the maximum displacement, acceleration, drift, and base shear of the structure and have sufficient strength against uncertainties. The primary aim of this study is to reduce the dynamic responses of the structure exposed to near-field and far-field earthquakes regardless of the structural system's dynamics and the information regarding the seismic input excitations. The ACNF controller is based on the neurochaotic fuzzy system in which an FOPID controller enhances its stability and robustness. The Jacobian of the system is extracted using the MLP neural network, whose coefficients are adaptive, and the structural system model is predicted. According to the extended Kalman filter and the error back-propagation method, the controller parameters are trained for adjusting the control force used in the ATMD. The ISAC controller is an improved simple adaptive controller whose parameters are optimized online by PSO as a novelty. As distinct from the fact that both controllers are regarded as novel adaptive controllers and have never been presented in the literature, their performance considerably outperforms the other state-of-the-art controllers based on the comparison findings. However, the ACNF controller by far precedes the ISAC controller in reducing the maximum displacement, acceleration, drift, and base shear. The significant conclusions obtained from the analysis of this research are summarized as follows:

(i) The ACNF controller performs better than the ISAC controller in mitigating the maximum displacement under the El Centro, Hachinohe, Kobe, and Northridge earthquakes by 16.5%, 15.5%, 17.1%, and 15.1% on average.

(ii) According to the findings, the RMS value obtained from the time history responses is lower in the ANCF controller than in the ISAC controller.

(iii) The ACNF controller outperforms the ISAC controller regarding the maximum acceleration reduction under the seismic excitations by 16.1% on the total average.

(iv) Another significant finding was that the ACNF controller showcased greater resilience in maintaining its exceptional performance under parametric uncertainties compared to the ISAC controller.

In conclusion, this study has provided valuable insights into the effectiveness of the ACNF and ISAC controllers in mitigating dynamic responses of structures subjected to earthquakes. The ACNF controller, with its neurochaotic fuzzy system and FOPID, proved to be a superior choice,

outperforming the ISAC controller in reducing maximum displacement and acceleration. Besides, this controller is able to tackle the uncertain parameters and the time-varying system successfully. This controller obtains a more accurate estimation of the structure's condition. These results contribute to the advancement of adaptive control strategies for enhancing the seismic resilience of structures. Further research can be conducted to explore additional applications and optimize the performance of these controllers in different scenarios.

Research in the future should examine the potential effects of using other neural networks more carefully; for example, using the emotional neural network (ENN) or RBF neural network rather than MLB neural network may lead to more accurate identification of systems. Furthermore, the online self-organizing fuzzy neural network (SOFNN) controller can perform as well as or better than the ACNF controller. In addition, we plan to consider deep learning neural networks in the future to provide a more efficient control algorithm than the ACNF controller. It may be possible to add an adaptive Type-2 Gaussian fuzzy PID controller or fractional-order type-3 fuzzy controller to the control system in the future in order to increase stability and robustness. An adaptive fuzzy sliding mode controller of type-2 can also be beneficial.

Also, future research in the field of adaptive control strategies for the seismic resilience of structures can build upon the findings and insights obtained from this study. Here are some suggestions for further investigation:

Comparative analysis: Conduct a more extensive comparative analysis of the ACNF and ISAC controllers with other adaptive control strategies, considering a wider range of seismic input excitations and structural systems. This would provide a comprehensive understanding of their performance and identify specific scenarios where each controller excels.

Controller optimization: Explore advanced optimization algorithms beyond the PSO used in the ISAC controller to enhance the performance of the controllers further. Techniques such as genetic algorithms, particle swarm optimization variants, or machine learning-based optimization algorithms could be employed to optimize the controller parameters for improved seismic response mitigation.

Nonlinear structures: Investigate the applicability and performance of the ACNF and ISAC controllers on nonlinear structures. Nonlinear systems pose additional challenges in adaptive control, and exploring how these controllers handle nonlinearities would be valuable for practical applications.

Real-time implementation: Evaluate the real-time implementation of the ACNF and ISAC controllers on physical structures. This would involve considering hardware constraints, communication delays, and practical limitations to assess the feasibility and effectiveness of these controllers in real-world scenarios.

Robustness analysis: Conduct a comprehensive robustness analysis of the ACNF and ISAC controllers to account for uncertainties in structural parameters, earthquake characteristics, and sensor measurements. Assessing the controllers' robustness to these uncertainties would provide insights into their reliability and resilience in practical applications.

Multiobjective optimization: Consider multiobjective optimization frameworks to simultaneously optimize multiple performance criteria, such as displacement, acceleration, and energy dissipation. This would enable the design of controllers that strike a balance between different objectives and offer more comprehensive control strategies.

Experimental validation: Perform experimental studies to validate the ACNF and ISAC controllers' performance in physical testing setups. This would provide empirical evidence of their effectiveness and practical applicability, further bolstering their credibility.

Other applications: Explore the ACNF and ISAC controllers' adaptability to other engineering applications beyond seismic resilience, such as wind-induced vibrations or structural control under extreme loading conditions. Assessing their performance in different contexts would broaden their scope and potential impact.

Data Availability

The data used to support the findings of this study are available from the corresponding author upon request.

Conflicts of Interest

The authors declare that they do not have any conflicts of interest.

Authors' Contributions

Ommegolsoum Jafarzadeh collected the definitions of intellectual content, developed the concepts, acquired the data, prepared the manuscript, performed the numerical studies, designed the study, analyzed the data, performed the statistical analysis, acquired the revision file, and edited the manuscript. Seyyed Arash Mousavi Ghasemi developed the concepts, performed the numerical studies, acquired the data, acquired the revision file, and edited the manuscript. Seyed Mehdi Zahrai developed the concepts, performed the numerical studies, acquired the data, acquired the revision

file, and edited the manuscript editing. Ardashir Mohammadzadeh designed the study and edited and reviewed the manuscript editing. Ramin Vafaei Poursorkhabi performed the literature search, acquired the data, and performed the statistical analysis.

References

[1] J. G. Chase, "Re-shaping hysteretic behaviour using semi-active resettable device dampers," *Engineering Structures*, vol. 28, no. 10, pp. 1418–1429, 2006.

[2] M. Bitaraf and L. R. Barroso, "Structural performance improvement using MR dampers with adaptive control method," in *Proceedings of the 2009 American Control Conference*, IEEE, New York, NY, USA, May 2009.

[3] M. Bitaraf, "Application of semi-active control strategies for seismic protection of buildings with MR dampers," *Engineering Structures*, vol. 32, no. 10, pp. 3040–3047, 2010.

[4] M. Bitaraf, S. Hurlebaus, and L. R. Barroso, "Active and semi-active adaptive control for undamaged and damaged building structures under seismic load," *Computer-Aided Civil and Infrastructure Engineering*, vol. 27, no. 1, pp. 48–64, 2012.

[5] M. Bitaraf and S. Hurlebaus, "Semi-active adaptive control of seismically excited 20-story nonlinear building," *Engineering Structures*, vol. 56, pp. 2107–2118, 2013.

[6] E. C. Tetila, "Detection and classification of soybean pests using deep learning with UAV images," *Computers and Electronics in Agriculture*, vol. 179, Article ID 105836, 2020.

[7] L. G. Van Willigenburg, J. D. Stigter, and J. Molenaar, "Sensitivity matrices as keys to local structural system properties of large-scale nonlinear systems," *Nonlinear Dynamics*, vol. 107, no. 3, pp. 2599–2618, 2022.

[8] P. Balaji and K. Karthik SelvaKumar, "Applications of nonlinearity in passive vibration control: a review," *Journal of Vibration Engineering and Technologies*, vol. 9, no. 2, pp. 183–213, 2021.

[9] A. Pippi, "Dynamic response to different models of adjacent coupled buildings," *Journal of Vibration Engineering and Technologies*, vol. 8, no. 1, pp. 247–256, 2020.

[10] R. W. Soares, L. R. Barroso, and O. A. Al-Fahdawi, "Response attenuation of cable-stayed bridge subjected to central US earthquakes using neuro-fuzzy and simple adaptive control," *Engineering Structures*, vol. 203, Article ID 109874, 2020.

[11] R. W Soares, L. R. Barroso, and O. As Al-Fahdawi, "Adaptive control for response attenuation of seismically excited cable-stayed bridges," *Journal of Vibration and Control*, vol. 26, no. 3-4, pp. 131–145, 2020.

[12] A. Andersson, A. O'Connor, and R. Karoumi, "Passive and adaptive damping systems for vibration mitigation and increased fatigue service life of a tied arch railway bridge," *Computer-Aided Civil and Infrastructure Engineering*, vol. 30, no. 9, pp. 748–757, 2015.

[13] M. Gutierrez Soto and H. Adeli, "Tuned mass dampers," *Archives of Computational Methods in Engineering*, vol. 20, no. 4, pp. 419–431, 2013.

[14] N. Fisco and H. Adeli, "Smart structures: part I—active and semi-active control," *Scientia Iranica*, vol. 18, no. 3, pp. 275–284, 2011.

[15] H. Kim and H. Adeli, "Wavelet-hybrid feedback linear mean squared algorithm for robust control of cable-stayed bridges," *Journal of Bridge Engineering*, vol. 10, no. 2, pp. 116–123, 2005.

[16] E. Nazarimofrad and S. M. Zahrai, "Fuzzy control of asymmetric plan buildings with active tuned mass damper considering soil-structure interaction," *Soil Dynamics and Earthquake Engineering*, vol. 115, pp. 838–852, 2018.

[17] M. G. Soto and H. Adeli, "Placement of control devices for passive, semi-active, AND active vibration control of structures," *Scientia Iranica*, vol. 20, no. 6, pp. 1567–1578, 2013.

[18] A.-A. Zamani and S. Etedali, "Optimal fractional-order PID control design for time-delayed multi-input multi-output seismic-excited structural system," *Journal of Vibration and Control*, vol. 29, no. 3-4, pp. 802–819, 2023.

[19] A.-A. Zamani and S. Etedali, "Seismic response prediction of open-and closed-loop structural control systems using a multi-state-dependent parameter estimation approach," *International Journal of Computational Methods*, vol. 19, no. 5, Article ID 2250006, 2022.

[20] N. Fisco and H. Adeli, "Smart structures: part II—hybrid control systems and control strategies," *Scientia Iranica*, vol. 18, no. 3, pp. 285–295, 2011.

[21] H. Kim and H. Adeli, "Hybrid control of smart structures using a novel wavelet-based algorithm," *Computer-Aided Civil and Infrastructure Engineering*, vol. 20, no. 1, pp. 7–22, 2005.

[22] O. El-Khoury and H. Adeli, "Recent advances on vibration control of structures under dynamic loading," *Archives of Computational Methods in Engineering*, vol. 20, no. 4, pp. 353–360, 2013.

[23] E. Nazarimofrad and S. M. Zahrai, "Seismic control of irregular multistory buildings using active tendons considering soil–structure interaction effect," *Soil Dynamics and Earthquake Engineering*, vol. 89, pp. 100–115, 2016.

[24] M. Soleymani, "Modified sliding mode control of a seismic active mass damper system considering model uncertainties and input time delay," *Journal of Vibration and Control*, vol. 24, no. 6, pp. 1051–1064, 2018.

[25] N. Anh and N. Nguyen, "Design of TMD for damped linear structures using the dual criterion of equivalent linearization method," *International Journal of Mechanical Sciences*, vol. 77, pp. 164–170, 2013.

[26] S. Etedali, M. Akbari, and M. Seifi, "MOCS-based optimum design of TMD and FTMD for tall buildings under near-field earthquakes including SSI effects," *Soil Dynamics and Earthquake Engineering*, vol. 119, pp. 36–50, 2019.

[27] A.-A. Zamani and S. Etedali, "New formulas for optimal design of TMD using genetic programming method and their application to control of seismic-excited structures," *Journal of Structural and Construction Engineering*, vol. 10, no. 4, 2023.

[28] Z. Lu, X. Lu, and S. F. Masri, "Studies of the performance of particle dampers under dynamic loads," *Journal of Sound and Vibration*, vol. 329, no. 26, pp. 5415–5433, 2010.

[29] Z. Lu, "Nonlinear dissipative devices in structural vibration control: a review," *Journal of Sound and Vibration*, vol. 423, pp. 18–49, 2018.

[30] Z. Lu, "Experimental and numerical study on the dynamic behavior of a semi-active impact damper," *Smart Structures and Systems*, vol. 31, no. 5, pp. 455–467, 2023.

[31] H. Ren, Q. Fan, and Z. Lu, "Shaking table test and parameter analysis on vibration control of a new damping system (PDAL)," *Buildings*, vol. 12, no. 7, p. 896, 2022.

[32] K. Rong and Z. Lu, "An improved ESM-FEM method for seismic control of particle tuned mass damper in MDOF system," *Applied Acoustics*, vol. 172, Article ID 107663, 2021.

[33] F. Sadek, "A method of estimating the parameters of tuned mass dampers for seismic applications," *Earthquake Engineering and Structural Dynamics*, vol. 26, no. 6, pp. 617–635, 1997.

[34] S. Nagarajaiah, "Adaptive passive, semiactive, smart tuned mass dampers: identification and control using empirical mode decomposition, Hilbert transform, and short-term Fourier transform," *Structural Control and Health Monitoring*, vol. 16, no. 7, pp. 800–841, 2009.

[35] J. C. Miranda, "Discussion of system intrinsic parameters of tuned mass dampers used for seismic response reduction," *Structural Control and Health Monitoring*, vol. 23, no. 2, pp. 349–368, 2016.

[36] M. Abé and Y. Fujino, "Dynamic characterization of multiple tuned mass dampers and some design formulas," *Earthquake Engineering and Structural Dynamics*, vol. 23, no. 8, pp. 813–835, 1994.

[37] C. Li, "Performance of multiple tuned mass dampers for attenuating undesirable oscillations of structures under the ground acceleration," *Earthquake Engineering and Structural Dynamics*, vol. 29, no. 9, pp. 1405–1421, 2000.

[38] C. Li and W. Qu, "Optimum properties of multiple tuned mass dampers for reduction of translational and torsional response of structures subject to ground acceleration," *Engineering Structures*, vol. 28, no. 4, pp. 472–494, 2006.

[39] A. Bathaei, S. M. Zahrai, and M. Ramezani, "Semi-active seismic control of an 11-DOF building model with TMD+MR damper using type-1 and-2 fuzzy algorithms," *Journal of Vibration and Control*, vol. 24, no. 13, pp. 2938–2953, 2018.

[40] F. Rahimi, R. Aghayari, and B. Samali, "Application of tuned mass dampers for structural vibration control: a state-of-the-art review," *Civil Engineering Journal*, vol. 6, no. 8, pp. 1622–1651, 2020.

[41] W. Yu and S. Thenozhi, *Active Structural Control with Stable Fuzzy PID Techniques*, Springer, Berlin, Germany, 2016.

[42] Q. Li, "Optimal design of wind-induced vibration control of tall buildings and high-rise structures," *Wind and Structures*, vol. 2, no. 1, pp. 69–83, 1999.

[43] S. Pourzeynali, H. Lavasani, and A. Modarayi, "Active control of high rise building structures using fuzzy logic and genetic algorithms," *Engineering Structures*, vol. 29, no. 3, pp. 346–357, 2007.

[44] F. Amini and K. Karami, "Capacity design by developed pole placement structural control," *Structural Engineering and Mechanics*, vol. 39, no. 1, pp. 147–168, 2011.

[45] C. Collette and S. Chesne, "Robust hybrid mass damper," *Journal of Sound and Vibration*, vol. 375, pp. 19–27, 2016.

[46] Y. Xu, H. Hua, and J. Han, "Modeling and controller design of a shaking table in an active structural control system," *Mechanical Systems and Signal Processing*, vol. 22, no. 8, pp. 1917–1923, 2008.

[47] C. Li, J. Li, and Y. Qu, "An optimum design methodology of active tuned mass damper for asymmetric structures," *Mechanical Systems and Signal Processing*, vol. 24, no. 3, pp. 746–765, 2010.

[48] S. Etedali and S. Tavakoli, "PD/PID controller design for seismic control of high-rise buildings using multi-objective optimization: a comparative study with LQR controller," *Journal of Earthquake and Tsunami*, vol. 11, no. 3, Article ID 1750009, 2017.

[49] S. Park, "Numerical and experimental investigation of control performance of active mass damper system to high-rise building in use," *Wind and Structures An International Journal*, vol. 12, no. 4, pp. 313–332, 2009.

[50] L. Huo, "Robust control design of active structural vibration suppression using an active mass damper," *Smart Materials and Structures*, vol. 17, no. 1, Article ID 015021, 2007.

[51] R. Collins, B. Basu, and B. Broderick, "Control strategy using bang–bang and minimax principle for FRF with ATMDs," *Engineering Structures*, vol. 28, no. 3, pp. 349–356, 2006.

[52] E. Talib, J.-H. Shin, and M. K. Kwak, "Designing multi-input multi-output modal-space negative acceleration feedback control for vibration suppression of structures using active mass dampers," *Journal of Sound and Vibration*, vol. 439, pp. 77–98, 2019.

[53] D.-H. Yang, "Active vibration control of structure by active mass damper and multi-modal negative acceleration feedback control algorithm," *Journal of Sound and Vibration*, vol. 392, pp. 18–30, 2017.

[54] B.-L. Zhang, "Optimal tracking control with feedforward compensation for offshore steel jacket platforms with active mass damper mechanisms," *Journal of Vibration and Control*, vol. 22, no. 3, pp. 695–709, 2016.

[55] N. Mamat, "Seismic vibration suppression of a building with an adaptive nonsingular terminal sliding mode control," *Journal of Vibration and Control*, vol. 26, no. 23-24, pp. 2136–2147, 2020.

[56] M. Khatibinia, M. Mahmoudi, and H. Eliasi, "Optimal sliding mode control for seismic control of buildings equipped with ATMD," *International Journal of Optimization in Civil Engineering*, vol. 10, no. 1, pp. 1–15, 2020.

[57] A. Concha, "A tuning algorithm for a sliding mode controller of buildings with ATMD," 2020, https://arxiv.org/abs/2012.05966.

[58] R. Guclu and H. Yazici, "Seismic-vibration mitigation of a nonlinear structural system with an ATMD through a fuzzy PID controller," *Nonlinear Dynamics*, vol. 58, no. 3, pp. 553–564, 2009.

[59] S. Thenozhi and W. Yu, "Active vibration control of building structures using fuzzy proportional-derivative/proportional-integral-derivative control," *Journal of Vibration and Control*, vol. 21, no. 12, pp. 2340–2359, 2015.

[60] S. Etedali, "Sensitivity analysis on optimal PID controller for nonlinear smart base-isolated structures," *International Journal of Structural Stability and Dynamics*, vol. 19, no. 7, Article ID 1950080, 2019.

[61] S. Etedali, A.-A. Zamani, and S. Tavakoli, "A GBMO-based PI λ D μ controller for vibration mitigation of seismic-excited structures," *Automation in Construction*, vol. 87, pp. 1–12, 2018.

[62] M. Azizi, "Optimum design of fuzzy controller using hybrid ant lion optimizer and Jaya algorithm," *Artificial Intelligence Review*, vol. 53, no. 3, pp. 1553–1584, 2020.

[63] S. Etedali and A.-A. Zamani, "Semi-active control of nonlinear smart base-isolated structures using MR damper: sensitivity and reliability analyses," *Smart Materials and Structures*, vol. 31, no. 6, Article ID 065021, 2022.

[64] A.-A. Zamani and S. Etedali, "Seismic structural control using magneto-rheological dampers: a decentralized interval type-2 fractional-order fuzzy PID controller optimized based on energy concepts," *ISA Transactions*, vol. 137, pp. 288–302, 2023.

[65] A.-A. Zamani and S. Etedali, "A new framework of multi-objective BELBIC for seismic control of smart base-isolated structures equipped with MR dampers," *Engineering with Computers*, vol. 38, no. 4, pp. 3759–3772, 2021.

[66] H. Shariatmadar, S. Golnargesi, and T. Akbarzadeh, *Vibration Control of Buildings Using ATMD against Earthquake Excitations through Interval Type-2 Fuzzy Logic Controller*, Springer, Berlin, Germany, 2014.

[67] A. Leung and H. Zhang, "Particle swarm optimization of tuned mass dampers," *Engineering Structures*, vol. 31, no. 3, pp. 715–728, 2009.

[68] L. Faravelli and T. Yao, "Use of adaptive networks in fuzzy control of civil structures," *Computer-Aided Civil and Infrastructure Engineering*, vol. 11, no. 1, pp. 67–76, 1996.

[69] Y. Ohtori, "Benchmark control problems for seismically excited nonlinear buildings," *Journal of Engineering Mechanics*, vol. 130, no. 4, pp. 366–385, 2004.

[70] M. Al-Dawod, "Fuzzy controller for seismically excited nonlinear buildings," *Journal of Engineering Mechanics*, vol. 130, no. 4, pp. 407–415, 2004.

[71] E.-G. Talbi, *Metaheuristics: From Design to Implementation*, John Wiley and Sons, Hoboken, NJ, USA, 2009.

[72] A. Kaveh, *Advances in Metaheuristic Algorithms for Optimal Design of Structures*, Springer, Berlin, Germany, 2014.

[73] A. Kaveh, *Applications of Metaheuristic Optimization Algorithms in Civil Engineering*, Springer, Berlin, Germany, 2017.

[74] A. Akbarimajd, S. Asefi, and H. Shayeghi, "Using Jaya algorithm to optimal tuning of LQR based power system stabilizers," in *Proceedings of the 2017 2nd IEEE International Conference on Computational Intelligence and Applications (ICCIA)*, Beijing, China, September 2017.

[75] C. Caraveo, F. Valdez, and O. Castillo, "Optimization of fuzzy controller design using a new bee colony algorithm with fuzzy dynamic parameter adaptation," *Applied Soft Computing*, vol. 43, pp. 131–142, 2016.

[76] H. A. Hashim, "Optimal tuning of fuzzy feedback filter for L1 adaptive controller using multi-objective particle swarm optimization for uncertain nonlinear MIMO systems," 2017, https://arxiv.org/abs/1710.05423.

[77] I. Venanzi, "A review on adaptive methods for structural control," *The Open Civil Engineering Journal*, vol. 10, no. 1, pp. 653–667, 2016.

[78] Z. Li and H. Adeli, "New discrete-time robust H2/H∞ algorithm for vibration control of smart structures using linear matrix inequalities," *Engineering Applications of Artificial Intelligence*, vol. 55, pp. 47–57, 2016.

[79] K. Sobel, H. Kaufman, and L. Mabius, "Implicit adaptive control for a class of MIMO systems," *IEEE Transactions on Aerospace and Electronic Systems*, vol. 5, pp. 576–590, 1982.

[80] M. U. Saeed, Z. Sun, and S. Elias, "Research developments in adaptive intelligent vibration control of smart civil structures," *Journal of Low Frequency Noise, Vibration and Active Control*, vol. 41, no. 1, pp. 292–329, 2021.

[81] P. Lu, S. Chen, and Y. Zheng, "Artificial intelligence in civil engineering," *Mathematical Problems in Engineering*, vol. 2012, Article ID 145974, 22 pages, 2012.

[82] Y. Chae, J. M. Ricles, and R. Sause, "Large-scale experimental studies of structural control algorithms for structures with magnetorheological dampers using real-time hybrid simulation," *Journal of Structural Engineering*, vol. 139, no. 7, pp. 1215–1226, 2013.

[83] Y. Lei, J. Lu, and J. Huang, "Integration of identification and vibration control of time-varying structures subject to unknown seismic ground excitation," *Journal of Vibration and Control*, vol. 26, no. 15-16, pp. 1330–1344, 2020.

[84] M. Lezgy-Nazargah, A. Elahi, and M. Pakizeh Tali, "H_∞ control method for seismically excited building structures with time-delay," *Journal of Vibration and Control*, vol. 26, no. 11-12, pp. 865–884, 2020.

[85] A. Yanik, U. Aldemir, and M. Bakioglu, "A new active control performance index for vibration control of three-dimensional structures," *Engineering Structures*, vol. 62-63, pp. 53–64, 2014.

[86] A. Mohammadzadeh and E. Kayacan, "A non-singleton type-2 fuzzy neural network with adaptive secondary membership for high dimensional applications," *Neurocomputing*, vol. 338, pp. 63–71, 2019.

[87] A. Dokht Shakibjoo, "A novel technique for load frequency control of multi-area power systems," *Energies*, vol. 13, no. 9, p. 2125, 2020.

[88] O. Castillo, "Type-2 fuzzy logic: theory and applications," in *Proceedings of the 2007 IEEE International Conference on Granular Computing (GRC 2007)*, San Jose, CA, USA, November 2007.

[89] O. Castillo, "High-speed interval type-2 fuzzy systems for dynamic parameter adaptation in harmony search for optimal design of fuzzy controllers," *Mathematics*, vol. 9, no. 7, p. 758, 2021.

[90] S. M. Hadad Baygi, "Development of a hybrid WOA-base fuzzy-PID for suppression of structure vibrations under seismic excitations," *AUT Journal of Mechanical Engineering*, vol. 5, no. 2, p. 1, 2021.

[91] S. Mohammadrezaei Nodeh, M. H. Ghasemi, and H. R. Mohammadi Daniali, "Hybrid control of fuzzy type 2-neural network and higher order sliding mode for robotic manipulator with parametric uncertainties and perturbations," *Journal of Mechanical Engineering*, vol. 51, no. 1, pp. 219–228, 2021.

[92] D. Sain and B. Mohan, "Modeling, simulation and experimental realization of a new nonlinear fuzzy PID controller using Center of Gravity defuzzification," *ISA Transactions*, vol. 110, pp. 319–327, 2021.

[93] S. Ulusoy, S. M. Nigdeli, and G. Bekdaş, "Novel metaheuristic-based tuning of PID controllers for seismic structures and verification of robustness," *Journal of Building Engineering*, vol. 33, Article ID 101647, 2021.

[94] H.-G. Han, "A self-organizing interval Type-2 fuzzy-neural-network for modeling nonlinear systems," *Neurocomputing*, vol. 290, pp. 196–207, 2018.

[95] C.-M. Lin, T.-L. Le, and T.-T. Huynh, "Self-evolving function-link interval type-2 fuzzy neural network for nonlinear system identification and control," *Neurocomputing*, vol. 275, pp. 2239–2250, 2018.

[96] D. Bhattacharya, A. Konar, and P. Das, "Secondary factor induced stock index time-series prediction using self-adaptive interval type-2 fuzzy sets," *Neurocomputing*, vol. 171, pp. 551–568, 2016.

[97] Q. Liu, J. Wang, and Z. Zeng, "Advances in neural networks, intelligent control and information processing," *Neurocomputing*, vol. 198, no. C, pp. 1–3, 2016.

[98] S. Golnargesi, H. Shariatmadar, and H. M. Razavi, "Seismic control of buildings with active tuned mass damper through interval type-2 fuzzy logic controller including soil–structure interaction," *Asian Journal of Civil Engineering*, vol. 19, no. 2, pp. 177–188, 2018.

[99] S. H. Hosseini Lavassani and S. Shangapour, "Interval type-2 fuzzy hybrid control of a high-rise building including soil–structure interaction under near-field and far-field ground motions," *Structural Engineering International*, vol. 32, no. 3, pp. 316–327, 2020.

[100] R. W. Soares, L. R. Barroso, and O. A. Al-Fahdawi, "Simple adaptive control to attenuate bridge's seismic responses considering parametric variations," *Advances in Structural Engineering*, vol. 23, no. 1, pp. 132–145, 2020.

[101] H. Mo, *Handbook of Research on Artificial Immune Systems and Natural Computing: Applying Complex Adaptive Technologies: Applying Complex Adaptive Technologies*, IGI Global, Pennsylvania, PA, USA, 2009.

[102] Z. Li, *Fuzzy Chaotic Systems*, Springer, Berlin, Germany, 2006.

[103] H. Korn and P. Faure, "Is there chaos in the brain? II. Experimental evidence and related models," *Comptes Rendus Biologies*, vol. 326, no. 9, pp. 787–840, 2003.

[104] M. Porto and P. Amato, "A fuzzy approach for modeling chaotic dynamics with assigned properties," in *Proceedings of the 9th IEEE International Conference on Fuzzy Systems. FUZZ-IEEE 2000*, San Antonio, TX, USA, January 2000.

[105] M. Tang, K. jun Wang, and Y. Zhang, "A research on chaotic recurrent fuzzy neural network and its convergence," in *Proceedings of the 2007 International Conference on Mechatronics and Automation*, Harbin, China, August 2007.

[106] J.-L. Meng, "Face recognition based on chaotic fuzzy RBF neural network," in *Proceedings of the 2008 International Conference on Intelligent Information Hiding and Multimedia Signal Processing*, IEEE, Harbin, China, August 2008.

[107] K. C. Schurter and P. N. Roschke, "Neuro-fuzzy control of structures using acceleration feedback," *Smart Materials and Structures*, vol. 10, no. 4, pp. 770–779, 2001.

[108] J. Wang and T. Kumbasar, "Parameter optimization of interval Type-2 fuzzy neural networks based on PSO and BBBC methods," *IEEE/CAA Journal of Automatica Sinica*, vol. 6, no. 1, pp. 247–257, 2019.

[109] M. Bozorgvar and S. M. Zahrai, "Semi-active seismic control of buildings using MR damper and adaptive neural-fuzzy intelligent controller optimized with genetic algorithm," *Journal of Vibration and Control*, vol. 25, no. 2, pp. 273–285, 2019.

[110] J. Tavoosi, M. A. Badamchizadeh, and S. Ghaemi, "Adaptive inverse control of nonlinear dynamical system using type-2 fuzzy neural networks," *Journal of control*, vol. 5, no. 2, pp. 52–60, 2011.

[111] A. C. Tolga, I. B. Parlak, and O. Castillo, "Finite-interval-valued Type-2 Gaussian fuzzy numbers applied to fuzzy TODIM in a healthcare problem," *Engineering Applications of Artificial Intelligence*, vol. 87, Article ID 103352, 2020.

[112] A.-A. Zamani and S. Etedali, "Robust output feedback-based neuro-fuzzy controller for seismically excited tall buildings with ATMD accounting for variations in the type of supporting soil," *Soil Dynamics and Earthquake Engineering*, vol. 164, Article ID 107614, 2023.

[113] R. Sabetahd, "Response attenuation of a structure equipped with ATMD under seismic excitations using methods of online simple adaptive controller and online adaptive type-2 neural-fuzzy controller," *Computational Intelligence and Neuroscience*, vol. 2022, Article ID 5832043, 25 pages, 2022.

[114] L. Koutsoloukas, N. Nikitas, and P. Aristidou, "Passive, semi-active, active and hybrid mass dampers: a literature review with associated applications on building-like structures," *Developments in the Built Environment*, vol. 12, Article ID 100094, 2022.

[115] A. Mohammadzadeh, "Training interval type-2 fuzzy systems based on error backpropagation," in *Modern Adaptive Fuzzy Control Systems*, Springer, Berlin, Germany, 2022.

[116] M. H. Wong, "The modeling of fuzzy systems based on LEE-Oscillatory Chaotic Fuzzy Model (LoCFM)," in *From Physics to Control through an Emergent View*, World Scientific, Singapore, 2010.

[117] L. A. Zadeh, "The concept of a linguistic variable and its application to approximate reasoning—I," *Information Sciences*, vol. 8, no. 3, pp. 199–249, 1975.

[118] N. N. Karnik, J. M. Mendel, and Q. Liang, "Type-2 fuzzy logic systems," *IEEE Transactions on Fuzzy Systems*, vol. 7, no. 6, pp. 643–658, 1999.

[119] S. F. Molaeezadeh and M. H. Moradi, "Neuro-chaotic fuzzy sets and systems," *Computational Intelligence in Electrical Engineering*, vol. 5, no. 1, pp. 41–56, 2014.

[120] C.-H. Wang, C.-S. Cheng, and T.-T. Lee, "Dynamical optimal training for interval type-2 fuzzy neural network (T2FNN)," *IEEE Transactions on Systems, Man, and Cybernetics, Part B (Cybernetics)*, vol. 34, no. 3, pp. 1462–1477, 2004.

[121] E. Chibuikem Nnadozie and O. Ukachukwu Oparaku, "Adaptation of a novel fuzzy logic controller to a hybrid renewable energy system," *Journal of Energy Research and Reviews*, vol. 8, pp. 1–10, 2018.

[122] H. A. Yousef, "Load frequency control of a multi-area power system: an adaptive fuzzy logic approach," *IEEE Transactions on Power Systems*, vol. 29, no. 4, pp. 1822–1830, 2014.

[123] R. Khezri, "An intelligent coordinator design for GCSC and AGC in a two-area hybrid power system," *Applied Soft Computing*, vol. 76, pp. 491–504, 2019.

[124] N. Chauhan, V. Ravi, and D. Karthik Chandra, "Differential evolution trained wavelet neural networks: application to bankruptcy prediction in banks," *Expert Systems with Applications*, vol. 36, no. 4, pp. 7659–7665, 2009.

[125] S. Kumarawadu and T. T. Lee, "Neuroadaptive combined lateral and longitudinal control of highway vehicles using RBF networks," *IEEE Transactions on Intelligent Transportation Systems*, vol. 7, no. 4, pp. 500–512, 2006.

[126] C.-H. Chen, C.-M. Lin, and T.-Y. Chen, "Intelligent adaptive control for MIMO uncertain nonlinear systems," *Expert Systems with Applications*, vol. 35, no. 3, pp. 865–877, 2008.

[127] C.-F. Hsu, "Adaptive fuzzy wavelet neural controller design for chaos synchronization," *Expert Systems with Applications*, vol. 38, no. 8, pp. 10475–10483, 2011.

[128] T. Zhao, "RBFN-based decentralized adaptive control of a class of large-scale non-affine nonlinear systems," *Neural Computing and Applications*, vol. 17, no. 4, pp. 357–364, 2008.

[129] D. Hanbay, I. Turkoglu, and Y. Demir, "An expert system based on wavelet decomposition and neural network for modeling Chua's circuit," *Expert Systems with Applications*, vol. 34, no. 4, pp. 2278–2283, 2008.

[130] F. Amini and M. Javanbakht, "Simple adaptive control of seismically excited structures with MR dampers," *Structural Engineering and Mechanics*, vol. 52, no. 2, pp. 275–290, 2014.

[131] I. Bar-Kana and H. Kaufman, "Simple adaptive control of large flexible space structures," *IEEE Transactions on Aerospace and Electronic Systems*, vol. 29, no. 4, pp. 1137–1149, 1993.

[132] S. Ulrich, A. Saenz-Otero, and I. Barkana, "Passivity-based adaptive control of robotic spacecraft for proximity operations under uncertainties," *Journal of Guidance, Control, and Dynamics*, vol. 39, no. 6, pp. 1444–1453, 2016.

[133] S. Lee and F. Kozin, "Bounded state control of linear structures," in *Structural Control*, Springer, Berlin, Germany, 1987.

[134] M. Bitaraf, L. R. Barroso, and S. Hurlebaus, "Adaptive control to mitigate damage impact on structural response," *Journal of Intelligent Material Systems and Structures*, vol. 21, no. 6, pp. 607–619, 2010.

[135] I. Bar-Kana and A. Guez, "*Simplified techniques for adaptive control of robotic systems.* Control dyn syst V40: adv robot syst Part 2 of 2," *Advanced Theory and Simulations*, vol. 40, p. 147, 2012.

[136] A. Hosseini, T. Taghikhany, and A. Yeganeh Fallah, "Direct adaptive algorithm for seismic control of damaged structures with faulty sensors," *Journal of Vibration and Control*, vol. 24, no. 24, pp. 5854–5866, 2018.

[137] A. Hosseini and T. Taghikhany, "Online self-tuning mechanism for direct adaptive control of tall building," *International Journal of Adaptive Control and Signal Processing*, vol. 32, no. 3, pp. 424–446, 2018.

[138] H. Klee and R. Allen, Simulation of dynamic systems with MATLAB® and Simulink®, Crc Press, 2018.